Journal of Computational Physics 405 (2020) 109109

Contents lists available at ScienceDirect

Journal of Computational Physics

www.elsevier.com/locate/jcp

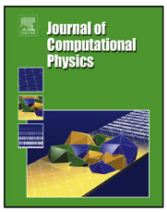

A weakly nonlinear, energy stable scheme for the strongly anisotropic Cahn-Hilliard equation and its convergence analysis

Kelong Cheng [a], Cheng Wang [b], Steven M. Wise [c,*]

[a] School of Science, Southwest University of Science and Technology, Mianyang, Sichuan 621010, PR China
[b] Department of Mathematics, The University of Massachusetts, North Dartmouth, MA 02747, USA
[c] Department of Mathematics, The University of Tennessee, Knoxville, TN 37996, USA

ARTICLE INFO

Article history:
Received 7 June 2019
Received in revised form 27 September 2019
Accepted 6 November 2019
Available online 19 November 2019

Keywords:
Anisotropic Cahn-Hilliard equation
Convexity analysis
Energy stability
Optimal rate convergence analysis
Biharmonic regularization
Fourier pseudo-spectral approximation

ABSTRACT

In this paper we propose and analyze a weakly nonlinear, energy stable numerical scheme for the strongly anisotropic Cahn-Hilliard model. In particular, a highly nonlinear and singular anisotropic surface energy makes the PDE system very challenging at both the analytical and numerical levels. To overcome this well-known difficulty, we perform a convexity analysis on the anisotropic interfacial energy, and a careful estimate reveals that all its second order functional derivatives stay uniformly bounded by a global constant. This subtle fact enables one to derive an energy stable numerical scheme. Moreover, a linear approximation becomes available for the surface energy part, and a detailed estimate demonstrates the corresponding energy stability. Its combination with an appropriate treatment for the nonlinear double well potential terms leads to a weakly nonlinear, energy stable scheme for the whole system. In particular, such an energy stability is in terms of the interfacial energy with respect to the original phase variable, and no auxiliary variable needs to be introduced. This has important implications, for example, in the case that the method needs to satisfy a maximum principle. More importantly, with a careful application of the global bound for the second order functional derivatives, an optimal rate convergence analysis becomes available for the proposed numerical scheme, which is the first such result in this area. Meanwhile, for a Cahn-Hilliard system with a sufficiently large degree of anisotropy, a Willmore or biharmonic regularization has to be introduced to make the equation well-posed. For such a physical model, all the presented analyses are still available; the unique solvability, energy stability and convergence estimate can be derived in an appropriate manner. In addition, the Fourier pseudo-spectral spatial approximation is applied, and all the theoretical results could be extended for the fully discrete scheme. Finally, a few numerical results are presented, which confirm the robustness and accuracy of the proposed scheme.

* Corresponding author.

1. Introduction

The Cahn-Hilliard flow, which models spinodal decomposition and phase separation in a binary alloy [5,6], is one of the best known PDEs of gradient flow type. In the Cahn-Hilliard family of models, sharp interfaces are replaced by narrow diffusive transition layers, which often leads to models that are simpler and more theoretically tractable than their sharp interface counterparts. In crystalline solids, the energy of interfaces can change according to the orientation of that interface. In fact, the energy of certain orientations may be large enough so that they do not naturally appear in the microstructure. In the sharp interface case, when the surface energy density is a smooth function of the interface normal and the anisotropy is sufficiently strong, it is known that there are missing orientations in the Wulff shape, that is, the shape that minimizes the total surface energy for a given volume [7,47]. Crystalline anisotropy plays a very important role in the material properties of heterogeneous solids. In the absence of anisotropy, microscopic precipitates are expected to be rotationally symmetric. Anisotropy breaks this symmetry as certain directions are endowed with higher free energy.

Here, we consider a bounded domain $\Omega \subset \mathbb{R}^d$, $d = 2, 3$. By ϕ we denote the phase variable (order parameter), and we set $\boldsymbol{p} := \nabla\phi$. The vector $\boldsymbol{n} := \frac{\boldsymbol{p}}{|\boldsymbol{p}|}$ is the unit normal vector with respect to iso-contours of ϕ, having the components

$$n_i = \frac{\partial_{x_i}\phi}{|\nabla\phi|} = \frac{p_i}{|\boldsymbol{p}|}, \quad i = 1, \cdots, d.$$

Of course, the normal vector is defined everywhere that $\nabla\phi$ is non-zero. The following anisotropic Kobayashi-type [41] free energy is proposed for consideration:

$$E(\phi) = \int_\Omega \left(\frac{1}{4}(\phi^2 - 1)^2 + \frac{\varepsilon^2}{2}\gamma^2(\boldsymbol{n})|\boldsymbol{p}|^2 \right) d\boldsymbol{x}, \quad \gamma(\boldsymbol{n}) = 1 + \alpha\Gamma(\boldsymbol{n}), \tag{1.1}$$

where ε is an interface transition width parameter, $f(\phi) = \frac{1}{4}(\phi^2 - 1)^2$ is a double well potential, $\gamma(\boldsymbol{n})$ is the interfacial energy function describing the nature of the anisotropy, and $\alpha \geq 0$ is the anisotropy strength. For four-fold anisotropy, a common choice for the anisotropy structure function, Γ, is

$$\Gamma(\boldsymbol{n}) = \Gamma_4(\boldsymbol{n}) := 4\sum_{i=1}^{d} n_i^4 - 3. \tag{1.2}$$

Here we will mainly focus on the four-fold case, though it is straightforward to generalize this to more exotic forms of anisotropy. In this model, the equilibrium profiles of one dimensional diffuse interfaces have different thicknesses, and, therefore, different energies, according to their orientation in space. In other words, the thickness of the interface is used to adjust the interfacial free energy as a function of orientation. This is in contrast to the model in Torabi *et al.* [51], where the equilibrium thickness does not change with orientation. However, the latter model is much more nonlinear than the one considered and may be the subject of a future study.

In the present model (1.1) the primary difference between isotropic and anisotropic systems is the structure of the $\gamma(\boldsymbol{n})$ function. If $\gamma(\boldsymbol{n}) \equiv 1$ (or equivalently, $\alpha = 0$), one recovers the isotropic model, which leads to the standard Cahn-Hilliard equation in the H^{-1} flow. The anisotropy function presented in (1.1) has been studied in [47] and elsewhere. For small values of α, the gradient free energy density function

$$\mathcal{G}(\boldsymbol{p}) := \gamma^2\left(\frac{\boldsymbol{p}}{|\boldsymbol{p}|}\right)|\boldsymbol{p}|^2$$

remains a convex function of $\boldsymbol{p}$. (Of course, it is convex when $\alpha = 0$.) However, for sufficiently large values of α, it is possible that $\mathcal{G}(\boldsymbol{p})$ can become indeterminate, non-convex and non-concave. In this case, we say that we are in the *strong anisotropy* regime. There is a simple test in two dimensions to determine the strong anisotropy regime with precision. In the two-dimensional setting, where θ denotes the angle between the normal vector $\boldsymbol{n}$ and $\boldsymbol{e}_1$, the canonical basis vector pointing in the x-direction, the interfacial energy function can be rewritten as $\gamma(\boldsymbol{n}) = \tilde{\gamma}(\theta) := 1 + \alpha\tilde{\Gamma}(\theta)$. When $\tilde{\gamma}(\theta) + \tilde{\gamma}''(\theta) < 0$, for some angles of θ [56], the problem is strongly anisotropic. There will be missing orientations (angles) on the equilibrium (Wulff) shape [56]. In the case of four-fold anisotropy, $\tilde{\Gamma}(\theta) = \cos(4\theta)$, and, if $\gamma > \frac{1}{15}$, then we are in the strongly anisotropic regime.

Define the projection matrix $\mathbf{P} := \mathbf{I} - \boldsymbol{n} \otimes \boldsymbol{n}$, where $\mathbf{I}$ is the identity matrix. Let us suppose, for simplicity that ϕ is Ω-periodic. The corresponding anisotropic Cahn-Hilliard system becomes the corresponding H^{-1} flow:

$$\partial_t\phi = \Delta\mu, \quad \mu = \phi^3 - \phi - \varepsilon^2\nabla\cdot\left(\gamma^2(\boldsymbol{n})\nabla\phi + \gamma(\boldsymbol{n})|\nabla\phi|\mathbf{P}\nabla_n\gamma(\boldsymbol{n})\right), \tag{1.3}$$

There have been quite a few existing numerical works for the anisotropic Cahn-Hilliard model, such as [28], where the authors use a convexification technique and [10,56], whose authors use a stabilized time discretizations, with adaptive finite difference multigrid solvers. Because of the highly singular nature of the surface energy, a theoretical justification of the energy stability turns out to be a very challenging issue. A few recent works have addressed this subtle issue. For example, a convex splitting approach is proposed and analyzed in [17] for the anisotropic system with a Willmore regularization. On the other hand, a theoretical analysis for the energy stability is only available for the isotropic flow in [17]. A stabilized scalar auxiliary variable (SAV) approach is studied in more recent works [9,59] for the anisotropic flow, and a stability analysis has been provided for a numerically modified energy. However, we point out that a uniform in time bound for the energy functional (1.1), in terms of the original phase variable, is not theoretically available in this approach.

In this article, we propose and analyze a uniquely solvable, energy stable numerical scheme for the anisotropic Cahn-Hilliard system, with the stability in terms of the original energy functional (1.1). The key difficulty has always been associated with the highly nonlinear nature in the chemical potential of the surface energy part. To overcome this well-known difficulty, a careful convexity analysis is carried out for $\gamma(\boldsymbol{n})$, which reveals that all its second order functional derivatives stay uniformly bounded by a global constant. As a consequence, although the surface energy itself is a non-convex, non-concave functional, we are able to combine it with an artificial linear surface diffusion term, so that the combined functional could become either convex or concave. In particular, a combination with an artificial negative diffusion term makes it concave, which in turn leads to a linear approximation for the surface energy. Moreover, a careful analysis demonstrates the energy stability in terms of the original phase variable, and no auxiliary variable needs to be introduced. This approach avoids an implicit treatment of the nonlinear surface energy part, so that computational efficiency can be greatly improved. Meanwhile, a convex splitting method is applied to the double well potential terms, which in turn leads to a weakly nonlinear, energy stable scheme for the whole system.

In addition, the convergence analysis of any numerical scheme applied to the anisotropic Cahn-Hilliard system has been an open problem for a long time. In this article, we perform an optimal rate convergence analysis for the proposed numerical scheme, making use of a careful application of the global bound for the second order functional derivatives. To our knowledge, it will be the first such result in this area.

The anisotropic phase field equation may become ill-posed with increasing values of α. When the system becomes strongly anisotropic, we introduce a bi-harmonic regularization. For the regularized physical model, all the presented analyses are still available, including the unique solvability, energy stability and convergence estimates.

For simplicity of presentation, we choose the Fourier pseudo-spectral spatial approximation. The advantage of this discretization is associated with the fact all the numerical variables, such as the phase variable, its gradient, and the Laplacian one, are evaluated at the regular grid points; no staggered finite difference mesh points are needed in the numerical implementation [17,56]. Moreover, the summation by parts formulae enable us to extend all the theoretical results to the fully discrete scheme, including the unique solvability, energy stability (in terms of the original phase variable), and optimal rate convergence estimates.

This paper is organized as follows. In Section 2, we provide a convexity analysis for the surface diffusion coefficients. The numerical scheme is formulated in Section 3, where the unique solvability and energy stability are established. An optimal rate convergence analysis is presented in Section 4. The numerical approximation for the strongly anisotropic system (with missing orientations on the Wulff shape) is considered in Section 5, in which a bi-harmonic regularization is added. All the theoretical results are established for this case as well. The Fourier pseudo-spectral approximation is reviewed, and the fully discrete scheme is outlined in Section 6. Some numerical results are presented in Section 7, and concluding remarks are made in Section 8.

2. Convexity analysis for the physical energy

The key difficulty to derive an energy stable scheme for the anisotropic CH model is associated with the highly singular and nonlinear nature of $\gamma(\boldsymbol{n})$. To overcome this difficulty, we have to obtain a convexity analysis for the energy functional (1.1). In particular, we focus on the surface diffusion energy functional $\int_\Omega \mathcal{G}(\boldsymbol{p})\, d\boldsymbol{x}$. It turns out that, in general, this is a non-convex, non-concave, highly singular term.

As stated earlier, we work specifically with the four-fold anisotropy function

$$\gamma(\boldsymbol{n}) = 1 - 3\alpha + 4\alpha(n_1^4 + n_2^4 + n_3^4).$$

The eight-fold anisotropy function, for example would be treated similarly, though the precise details will differ. For the four-fold function, we begin with the following observation:

$$\nu^2(\boldsymbol{n}) = (1-3\alpha)^2 + 8\alpha(1-3\alpha)\frac{p_1^4 + p_2^4 + p_3^4}{\quad} + 16\alpha^2\frac{(p_1^4 + p_2^4 + p_3^4)^2}{\quad}. \tag{2.1}$$

where

$$g^{(1)}(\boldsymbol{p}) := \frac{p_1^4+p_2^4+p_3^4}{p_1^2+p_2^2+p_3^2}, \quad g^{(2)}(\boldsymbol{p}) := \frac{(p_1^4+p_2^4+p_3^4)^2}{(p_1^2+p_2^2+p_3^2)^3}. \tag{2.3}$$

A direct calculation gives the first order derivatives of $g^{(1)}$ and $g^{(2)}$:

$$\partial_{p_i} g^{(1)}(\boldsymbol{p}) = \frac{4p_i^3 \sum_{j=1}^3 p_j^2 - 2p_i \sum_{j=1}^3 p_j^4}{\left(\sum_{j=1}^3 p_j^2\right)^2}, \quad i=1,2,3, \tag{2.4}$$

$$\partial_{p_i} g^{(2)}(\boldsymbol{p}) = \frac{2p_i \sum_{j=1}^3 p_j^4 \left(4p_i^2 \sum_{j=1}^3 p_j^2 - 3\sum_{j=1}^3 p_j^4\right)}{\left(\sum_{j=1}^3 p_j^2\right)^4}, \quad i=1,2,3. \tag{2.5}$$

Furthermore, the following lemma is needed in the convexity analysis; the proof will be given in Appendix A.

Lemma 2.1. *Define*

$$D_1^{(1)} := \frac{7}{2}, \quad D_2^{(1)} := 2, \quad D_1^{(2)} := 6, \quad D_2^{(2)} := 3.$$

The functions $g^{(1)}$, $g^{(2)}$, are twice continuously differentiable in $\mathbb{R}^3_\star := \mathbb{R}^3 \setminus \{\mathbf{0}\}$, and we have the bounds

$$|\partial^2_{p_i} g^{(1)}(\boldsymbol{p})| \le D_1^{(1)}, \quad i=1,2,3, \qquad |\partial_{p_i}\partial_{p_j} g^{(1)}(\boldsymbol{p})| \le D_2^{(1)}, \quad i,j=1,2,3,\ i\neq j, \tag{2.6}$$

$$|\partial^2_{p_i} g^{(2)}(\boldsymbol{p})| \le D_1^{(2)}, \quad i=1,2,3, \qquad |\partial_{p_i}\partial_{p_j} g^{(2)}(\boldsymbol{p})| \le D_2^{(2)}, \quad i,j=1,2,3,\ i\neq j, \tag{2.7}$$

for all $\boldsymbol{p} \in \mathbb{R}^3_\star$.

Let us denote by $\mathbf{G}^{(1)}$ and $\mathbf{G}^{(2)}$ the Hessian matrices associated with the scalar functions $g^{(1)}$, $g^{(2)}$, respectively. The following result is available.

Corollary 2.2. *Define*

$$\mathbf{H}^{(k)} := \mathbf{G}^{(k)} + B_0^{(k)}\mathbf{I}, \quad k=1,2.$$

Then $\mathbf{H}^{(1)}$ and $\mathbf{H}^{(2)}$ are non-negative definite in $\mathbb{R}^3_\star = \mathbb{R}^3 \setminus \{\mathbf{0}\}$, provided $B_0^{(1)} \ge \frac{15}{2}$ and $B_0^{(2)} \ge 12$.

Proof. It is clear that

$$\mathbf{H}^{(k)} = \begin{pmatrix} g_{1,1}^{(k)} + B_0^{(k)} & g_{1,2}^{(k)} & g_{1,3}^{(k)} \\ g_{2,1}^{(k)} & g_{2,2}^{(k)} + B_0^{(k)} & g_{2,3}^{(k)} \\ g_{3,1}^{(k)} & g_{3,2}^{(k)} & g_{3,3}^{(k)} + B_0^{(k)} \end{pmatrix}, \quad k=1,2,$$

where, for brevity, $g_{i,j}^{(k)} := \partial_{p_i}\partial_{p_j} g^{(k)}$. For the matrix $\mathbf{H}^{(1)}$, we see that

$$g_{1,1}^{(1)} + B_0^{(1)} \ge B_0^{(1)} - |g_{1,1}^{(1)}| \ge \frac{15}{2} - \frac{7}{2} = 4 \ge |g_{1,2}^{(1)}| + |g_{1,3}^{(1)}|, \tag{2.8}$$

in which estimate (2.6) of Lemma 2.1 has been used. Similar estimates could be derived for the second and third rows:

$$g_{2,2}^{(1)} + B_0^{(1)} \ge |g_{2,1}^{(1)}| + |g_{2,3}^{(1)}|, \quad g_{3,3}^{(1)} + B_0^{(1)} \ge |g_{3,1}^{(1)}| + |g_{3,2}^{(1)}|. \tag{2.9}$$

Therefore, the matrix $\mathbf{H}^{(1)}$ is diagonally dominant. Since it is also symmetric, it must be non-negative definite.

In a similar way, we can prove that $\mathbf{H}^{(2)}$ is diagonally dominant and, therefore, non-negative definite. The details are left to interested readers. □

We immediately have the following corollary.

On the other hand, based on the detailed expansions in (2.4) and (2.5), we observe that, while $g^{(1)}, g^{(2)} \in C^1(\mathbb{R}^3)$, these functions are not twice differentiable at $\mathbf{0}$. The Hessian matrices defined above are not well-defined at $\mathbf{0}$. To overcome this difficulty, the following lemma is needed to treat the singularity at $\mathbf{0}$.

Lemma 2.4. *Assume that $f \in C^1(\mathbb{R}^3)$ satisfies the following property: $f \in C^2(\mathbb{R}^3_\star)$ and its Hessian matrix $\mathbf{S}$ is non-negative definite in $\mathbb{R}^3_\star = \mathbb{R}^3 \setminus \{\mathbf{0}\}$. Then f is convex over $\mathbb{R}^3$, and, consequently,*

$$f\Big(\frac{\boldsymbol{x}_1+\boldsymbol{x}_2}{2}\Big) \le \frac{1}{2}\Big(f(\boldsymbol{x}_1)+f(\boldsymbol{x}_2)\Big), \quad \forall \boldsymbol{x}_1, \boldsymbol{x}_2 \in \mathbb{R}^3, \tag{2.10}$$

and

$$\nabla f(\boldsymbol{x}_2)\cdot(\boldsymbol{x}_2-\boldsymbol{x}_1) \ge f(\boldsymbol{x}_2)-f(\boldsymbol{x}_1), \quad \forall \boldsymbol{x}_1, \boldsymbol{x}_2 \in \mathbb{R}^3. \tag{2.11}$$

Proof. For any $\boldsymbol{x}_1, \boldsymbol{x}_2 \in \mathbb{R}^3$, define $L = |\boldsymbol{x}_2-\boldsymbol{x}_1|$ and $\mathbf{v} := \frac{\boldsymbol{x}_2-\boldsymbol{x}_1}{L}$ (so that $|\mathbf{v}|=1$). If the line segment from $\boldsymbol{x}_1$ to $\boldsymbol{x}_2$ – denoted $\overrightarrow{\boldsymbol{x}_1\boldsymbol{x}_2}$ – does not pass through the origin, $\mathbf{0}$, we see that f is smooth, with non-negative definite Hessian matrix over $\overrightarrow{\boldsymbol{x}_1\boldsymbol{x}_2}$, so that the directional derivative $D_{\mathbf{v}}f$ is increasing along the line segment $\overrightarrow{\boldsymbol{x}_1\boldsymbol{x}_2}$.

In the case that the vector $\overrightarrow{\boldsymbol{x}_1\boldsymbol{x}_2}$ does pass through $\mathbf{0}$, we parameterize this vector as follows: $\boldsymbol{x}_1 + t\mathbf{v}$, for $0 \le t \le L$, and define $L_1 := |\boldsymbol{x}_1|$. For any $\mathbf{y}$ along vector $\overrightarrow{\boldsymbol{x}_1\mathbf{0}}$, we denote $\mathbf{y}(t) = \boldsymbol{x}_1 + t\mathbf{v}$, for $0 \le t \le L_1$. By the Fundamental Theorem of Calculus the following identity is valid:

$$D_{\mathbf{v}}f(\mathbf{y}(t)) = D_{\mathbf{v}}f(\boldsymbol{x}_1) + \int_0^t D^2_{\mathbf{v}}f(\boldsymbol{x}_1+\xi\mathbf{v})\,d\xi, \quad \forall\, 0 \le t < L_1. \tag{2.12}$$

Furthermore, since $f \in C^1(\mathbb{R}^3)$,

$$D_{\mathbf{v}}f(\mathbf{0}) = D_{\mathbf{v}}f(\boldsymbol{x}_1) + \lim_{t \nearrow L_1}\int_0^t D^2_{\mathbf{v}}f(\boldsymbol{x}_1+\xi\mathbf{v})\,d\xi. \tag{2.13}$$

Since the Hessian matrix $\mathbf{S}$ is point-wise non-negative definite along the segment $\overrightarrow{\boldsymbol{x}_1\mathbf{0}}$ – not including the point $\mathbf{0}$ at which it may be undefined – we conclude that $D^2_{\mathbf{v}}f(\boldsymbol{x}_1+\xi\mathbf{v}) \ge 0$, for any $0 \le \xi < L_1$. This fact implies that

$$D_{\mathbf{v}}f(\mathbf{y}(t_2)) \ge D_{\mathbf{v}}f(\mathbf{y}(t_1)), \quad \text{for any} \quad 0 \le t_1 \le t_2 \le L_1. \tag{2.14}$$

In other words, $D_{\mathbf{v}}f$ is increasing along the segment $\overrightarrow{\boldsymbol{x}_1\mathbf{0}}$, from $\boldsymbol{x}_1$ all the way to $\mathbf{0}$.

A similar analysis could be carried out along vector $\overrightarrow{\mathbf{0}\boldsymbol{x}_2}$, so that

$$D_{\mathbf{v}}f(\mathbf{y}(t)) = D_{\mathbf{v}}f(\mathbf{0}) + \lim_{s \searrow L_1}\int_s^t D^2_{\mathbf{v}}f(\boldsymbol{x}_1+\xi\mathbf{v})\,d\xi, \quad \forall\, L_1 < t \le L. \tag{2.15}$$

We can conclude, using the non-negativity of the Hessian,

$$D_{\mathbf{v}}f(\mathbf{y}(t_2)) \ge D_{\mathbf{v}}f(\mathbf{y}(t_1)), \quad \text{for any} \quad L_1 \le t_1 \le t_2 \le L. \tag{2.16}$$

A combination of (2.14) and (2.16) indicates that $D_{\mathbf{v}}f$ is increasing all along the segment $\overrightarrow{\boldsymbol{x}_1\boldsymbol{x}_2}$:

$$D_{\mathbf{v}}f(\mathbf{y}(t_2)) \ge D_{\mathbf{v}}f(\mathbf{y}(t_1)), \quad \text{for any} \quad 0 \le t_1 \le t_2 \le L. \tag{2.17}$$

Since, $D_{\mathbf{v}}f$ is increasing along the segment $\overrightarrow{\boldsymbol{x}_1\boldsymbol{x}_2}$, for arbitrary $\boldsymbol{x}_1, \boldsymbol{x}_2 \in \mathbb{R}^3$, f must be convex, and the two inequalities in (2.11) become a straightforward consequence. □

Then we obtain the following convexity result.

Proposition 2.5. *Let $\alpha \ge 0$ be the anisotropy strength parameter. Define $E_S(\phi) := \int_\Omega \mathcal{G}(\boldsymbol{p})\,d\boldsymbol{x}$, $\boldsymbol{p} = \nabla\phi$. Then*

$$H_S(\phi) := E_S(\phi) + A_S\|\nabla\phi\|^2 \tag{2.18}$$

Proof. We define

$$\kappa(\boldsymbol{p}) := \mathcal{G}(\boldsymbol{p}) + A_1|\boldsymbol{p}|^2 = \Big((1-3\alpha)^2 + A_1\Big)|\boldsymbol{p}|^2 + 8\alpha(1-3\alpha)g^{(1)}(\boldsymbol{p}) + 16\alpha^2 g^{(2)}(\boldsymbol{p}). \tag{2.20}$$

For any $\boldsymbol{p} \in \mathbb{R}^3_\star$, the Hessian matrix of κ is precisely

$$\begin{aligned}\mathbf{K} &= 2\Big((1-3\alpha)^2 + A_1\Big)\mathbf{I} + 8\alpha(1-3\alpha)\mathbf{G}^{(1)} + 16\alpha^2\mathbf{G}^{(2)} \\ &\geq \begin{cases} 8\alpha|1-3\alpha|\mathbf{H}^{(1)} + 16\alpha^2\mathbf{H}^{(2)} & \text{if} \quad 1 \geq 3\alpha \\ 8\alpha|1-3\alpha|\mathbf{H}^{(3)} + 16\alpha^2\mathbf{H}^{(2)} & \text{if} \quad 1 \leq 3\alpha \end{cases}.\end{aligned} \tag{2.21}$$

Here, for symmetric matrices $\mathbf{A}$ and $\mathbf{B}$, $\mathbf{A} \geq \mathbf{B}$ means that $\mathbf{A}-\mathbf{B}$ is non-negative definite. Therefore, we conclude that the Hessian matrix $\mathbf{K}$ is non-negative definite over $\mathbb{R}^3_\star = \mathbb{R}^3 \setminus \{\mathbf{0}\}$, since $\mathbf{H}^{(1)}$, $\mathbf{H}^{(2)}$, $\mathbf{H}^{(3)}$ are non-negative definite (by Corollaries 2.2 and 2.3. In turn, with an application of Lemma 2.4, since $\kappa \in C^1(\mathbb{R}^3) \cup C^2(\mathbb{R}^3_\star)$, κ must be convex. Since $H_1(\phi) = \int_\Omega \kappa(\boldsymbol{p})\, d\boldsymbol{x}$, the convexity of the functional H_1 is assured. □

Remark 2.6. According to the last estimate, it follows that if $0 \leq \alpha \leq \alpha_o$, where

$$\alpha_o := \frac{36 - \sqrt{36^2 - 12}}{6} \approx 0.0278,$$

then we can take $A_1 = 0$ and still be assured that H_1 will be convex.

As a result of Proposition 2.5, the following convex-concave decomposition for the original energy functional $E(\phi)$ exists: define

$$E_c(\phi) := \int_\Omega \left(\frac{1}{4}\phi^4 + \frac{1}{4}\right) d\boldsymbol{x} + \frac{\varepsilon^2}{2}H_1(\phi) = \int_\Omega \left(\frac{1}{4}\phi^4 + \frac{1}{4} + \frac{\varepsilon^2}{2}(A_1 + \gamma^2(\boldsymbol{n}))|\nabla\phi|^2\right) d\boldsymbol{x}, \tag{2.22}$$

$$E_e(\phi) := \int_\Omega \left(\frac{1}{2}\phi^2 + \frac{A_1\varepsilon^2}{2}|\nabla\phi|^2\right) d\boldsymbol{x}. \tag{2.23}$$

Then $E = E_c - E_e$ and E_c and E_e are convex. It is then straightforward to devise a scheme that is unconditionally energy stable and unconditionally uniquely solvable using the framework devised in [57].

However, we observe that the highly nonlinear energy functional $E_S(\phi)$ is placed in the convex part in the decomposition (2.22) – (2.23), which would, in turn, lead to an implicit treatment of these nonlinear and singular terms. To overcome this well-known difficulty, we look for an alternate decomposition so that the nonlinear and singular expansions in the energy functional is placed in the concave part, whose terms would be treated explicitly in a numerical scheme. First, based on the expansion for $\mathcal{G}(\boldsymbol{p}) = \gamma^2(\boldsymbol{n})|\boldsymbol{p}|^2$ in (2.1), (2.2), and (2.3), we rewrite the surface free energy as

$$E_S(\phi) := \int_\Omega \mathcal{G}(\boldsymbol{p})\, d\boldsymbol{x} = (1-3\alpha)^2\|\nabla\phi\|^2 + \tilde{E}_S(\phi), \tag{2.24}$$

where the last term contains the nonlinear and singular terms:

$$\tilde{E}_S(\phi) := \int_\Omega \Big(8\alpha(1-3\alpha)g^{(1)}(\boldsymbol{p}) + 16\alpha^2 g^{(2)}(\boldsymbol{p})\Big) d\boldsymbol{x}, \quad \boldsymbol{p} = \nabla\phi. \tag{2.25}$$

Now, we define another functional:

$$H_2(\phi) := A_2\|\nabla\phi\|^2 - \tilde{E}_S(\phi) = \int_\Omega \Big(A_2|\boldsymbol{p}|^2 - 8\alpha(1-3\alpha)g^{(1)}(\boldsymbol{p}) - 16\alpha^2 g^{(2)}(\boldsymbol{p})\Big) d\boldsymbol{x}. \tag{2.26}$$

The following convexity result is available.

Proof. The convexity of H_2 can be proved by the same technique used previously. First, we define

$$\kappa(\boldsymbol{p}) = A_2|\boldsymbol{p}|^2 - 8\alpha(1-3\alpha)g^{(1)}(\boldsymbol{p}) - 16\alpha^2 g^{(2)}(\boldsymbol{p}). \tag{2.27}$$

Its Hessian matrix is

$$\begin{aligned}\mathbf{K} &= 2A_2\mathbf{I} - 8\alpha(1-3\alpha)\mathbf{G}^{(1)} - 16\alpha^2\mathbf{G}^{(2)} \\ &\geq 2\Big(4\alpha|1-3\alpha|B_0^{(1)} + 8\alpha^2 B_0^{(2)}\Big)\mathbf{I} - 8\alpha(1-3\alpha)\mathbf{G}^{(1)} - 16\alpha^2\mathbf{G}^{(2)} \\ &= \begin{cases} 8\alpha|1-3\alpha|\mathbf{H}^{(3)} + 16\alpha^2\mathbf{H}^{(4)} & \text{if} \quad 1 \geq 3\alpha \\ 8\alpha|1-3\alpha|\mathbf{H}^{(1)} + 16\alpha^2\mathbf{H}^{(4)} & \text{if} \quad 1 \leq 3\alpha \end{cases}. \end{aligned} \tag{2.28}$$

Making use of Corollaries 2.2 and 2.3, we conclude that $\mathbf{K}$ is non-negative definite in $\mathbb{R}^3_\star$. The result follows. □

As a result of Proposition 2.7, the following convex-concave decomposition for the original energy functional $E(\phi)$ becomes available.

Corollary 2.8. *The functionals*

$$E_c(\phi) = \int_\Omega \Big(\frac{1}{4}\phi^4 + \frac{1}{4} + \frac{\varepsilon^2}{2}((1-3\alpha) + A_2)|\nabla\phi|^2\Big)\, d\boldsymbol{x}, \tag{2.29}$$

$$E_e(\phi) = \frac{1}{2}\|\phi\|^2 + \frac{\varepsilon^2}{2}H_2(\phi) = \int_\Omega \Big(\frac{1}{2}\phi^2 + \frac{\varepsilon^2}{2}(-\tilde{E}_S(\phi) + A_2|\nabla\phi|^2)\Big)\, d\boldsymbol{x}, \tag{2.30}$$

are convex, provided $B_0^{(1)} \geq \frac{15}{2}$, $B_0^{(2)} \geq 12$, and $A_2 \geq 8\alpha^2 B_0^{(2)} + 4\alpha|1-3\alpha|B_0^{(1)}$. In other words, the energy $E(\phi)$ possesses a convex-concave decomposition, $E(\phi) = E_c(\phi) - E_e(\phi)$, using the alternate functionals (2.29) and (2.30).

We will need the functional derivative of $\tilde{E}_S$, which is

$$\delta_\phi \tilde{E}_S = -\nabla\cdot\Big((\gamma^2(\boldsymbol{n}) - (1-3\alpha)^2)\nabla\phi + \gamma(\boldsymbol{n})|\nabla\phi|\mathbf{P}\nabla_n\gamma(\boldsymbol{n})\Big). \tag{2.31}$$

As before, we are assuming Ω-periodic boundary conditions for ϕ. Based on the detailed expansion in (2.1), (2.2), and (2.3), this term could also be represented as

$$\begin{aligned}\delta_\phi \tilde{E}_S &= -\nabla\cdot\Big(8\alpha(1-3\alpha)\nabla_p g^{(1)}(\boldsymbol{p}) + 16\alpha^2\nabla_p g^{(2)}(\boldsymbol{p})\Big) \\ &:= -\nabla\cdot\left(8\alpha(1-3\alpha)\begin{pmatrix}\partial_{p_1} g^{(1)}(\boldsymbol{p}) \\ \partial_{p_2} g^{(1)}(\boldsymbol{p}) \\ \partial_{p_3} g^{(1)}(\boldsymbol{p})\end{pmatrix} + 16\alpha^2\begin{pmatrix}\partial_{p_1} g^{(2)}(\boldsymbol{p}) \\ \partial_{p_2} g^{(2)}(\boldsymbol{p}) \\ \partial_{p_3} g^{(2)}(\boldsymbol{p})\end{pmatrix}\right),\end{aligned} \tag{2.32}$$

where ∇_p is the gradient with respect to $\boldsymbol{p}$. The detailed expansions of $\partial_{p_i} g^{(j)}$, $i = 1,2,3$, $j = 1,2$, are given in (2.4) and (2.5).

Remark 2.9. In the convexity analysis, we focus on the four-fold anisotropy structure function (1.2) for simplicity of presentation. Of course, a more general structure function might be necessary for certain applications. For example, one may consider a function of the form

$$\gamma(\boldsymbol{n}) = \alpha_0 + \alpha_4\sum_{i=1}^d n_i^4 + \alpha_6\sum_{i=1}^d n_i^6 + \alpha_8\sum_{i=1}^d n_i^8 + \cdots, \tag{2.33}$$

where α_i, $i = 0,4,6,8,\cdots$, are constants. For this more general expression, the convexity analysis could be performed in a similar way. For example, in the expansion of $\gamma^2(\boldsymbol{n})$ the sixth-order term is expected to include a term in the form of

$$\frac{p_1^6 + p_2^6 + p_3^6}{(p_1^2 + p_2^2 + p_3^2)^3},$$

For $g^{(3)}$ and $g^{(4)}$, a uniform bound of the second order derivatives could be derived as in (2.6) and (2.7) in Lemma 2.1, with bounds $D_1^{(3)}$, $D_2^{(3)}$, $D_1^{(4)}$, $D_2^{(4)}$, being introduced. In turn, the convexity results stated in Propositions 2.5, 2.7 and Corollary 2.8 could be similarly established, but with modified values of A_1 and A_2.

3. A semi-discrete numerical scheme

A standard convex splitting scheme could be derived based on the alternate decomposition in (2.29) and (2.30) for the physical energy $E(\phi)$. On the other hand, such a convex splitting has to introduce artificial regularization term $-A_2\varepsilon^2\Delta(\phi^{n+1}-\phi^n)$, which may be large. To reduce the size of numerical dissipation, we consider the following semi-implicit, first-order-in-time numerical scheme:

$$\frac{\phi^{n+1}-\phi^n}{\Delta t} = \Delta\mu(\phi^{n+1},\phi^n), \tag{3.1}$$

$$\begin{aligned}\mu(\phi^{n+1},\phi^n) = {} & (\phi^{n+1})^3 - \phi^n - (1-3\alpha)^2\varepsilon^2\Delta\phi^{n+1} - \tilde{A}_2\varepsilon^2\Delta(\phi^{n+1}-\phi^n) \\ & -\varepsilon^2\nabla\cdot\Big(4\alpha(1-3\alpha)\nabla_p g^{(1)}(\nabla\phi^n) + 8\alpha^2\nabla_p g^{(2)}(\nabla\phi^n)\Big),\end{aligned} \tag{3.2}$$

with the artificial diffusion coefficient

$$\tilde{A}_2 = \max\Big(4\alpha^2 B_0^{(2)} + 2\alpha|1-3\alpha|B_0^{(1)} - \frac{1}{2}(1-3\alpha)^2, 0\Big) = \frac{A_1}{2},$$

where A_1 is given by (2.19). We observe that

$$\tilde{A}_2 = \frac{1}{2}\max(A_2 - (1-3\alpha)^2, 0) \le \frac{A_2}{2},$$

which would lead to half as much numerical dissipation. The following theoretical result is available by a careful energy analysis.

Theorem 3.1. *The proposed numerical scheme (3.1) and (3.2) is uniquely solvable and unconditionally energy stable: $E(\phi^{n+1}) \le E(\phi^n)$.*

Proof. The unique solvability of the scheme represented in (3.1) and (3.2) comes from a standard convexity analysis. In particular, the scheme results as the gradient of a strictly convex energy functional. The details are similar to what is described in [57] and in several other places.

In terms of the energy stability, we take an L^2 inner product of Equations (3.1) and (3.2) with $(-\Delta)^{-1}(\phi^{n+1}-\phi^n)$ and get

$$\begin{aligned}0 = {} & \Big((\phi^{n+1})^3, \phi^{n+1}-\phi^n\Big) - (\phi^n, \phi^{n+1}-\phi^n) + (1-3\alpha)^2\varepsilon^2(\nabla\phi^{n+1}, \nabla\left(\phi^{n+1}-\phi^n\right)) \\ & + \frac{1}{\Delta t}\|\phi^{n+1}-\phi^n\|_{\dot{H}^{-1}_{\rm per}}^2 + \tilde{A}_2\varepsilon^2\left\|\nabla\left(\phi^{n+1}-\phi^n\right)\right\|^2 \\ & -\varepsilon^2\Big(\nabla\cdot\Big(4\alpha(1-3\alpha)\nabla_p g^{(1)}(\nabla\phi^n) + 8\alpha^2\nabla_p g^{(2)}(\nabla\phi^n)\Big), \phi^{n+1}-\phi^n\Big),\end{aligned} \tag{3.3}$$

using integration-by-parts. The following convexity estimates/identies are valid:

$$\Big((\phi^{n+1})^3, \phi^{n+1}-\phi^n\Big) \ge \frac{1}{4}\Big(\int_\Omega (\phi^{n+1})^4\,d\boldsymbol{x} - \int_\Omega (\phi^n)^4\,d\boldsymbol{x}\Big), \tag{3.4}$$

$$\left(-\phi^n, \phi^{n+1}-\phi^n\right) \ge -\frac{1}{2}\Big(\int_\Omega (\phi^{n+1})^2\,d\boldsymbol{x} - \int_\Omega (\phi^n)^2\,d\boldsymbol{x}\Big), \tag{3.5}$$

$$(\nabla\phi^{n+1}, \nabla\left(\phi^{n+1}-\phi^n\right)) = \frac{1}{2}(\|\nabla\phi^{n+1}\|^2 - \|\nabla\phi^n\|^2) + \frac{1}{2}\|\nabla(\phi^{n+1}-\phi^n)\|^2. \tag{3.6}$$

For the nonlinear surface diffusion terms, we make use of the convexity property of H_2, as given by Proposition 2.7

$$-\left(\delta_\phi H_2(\phi^n), \phi^{n+1}-\phi^n\right) \ge -(H_2(\phi^{n+1}) - H_2(\phi^n)). \tag{3.7}$$

Meanwhile, by the following identity

$$2A_2(\Delta\phi^n, \phi^{n+1}-\phi^n) = -A_2(\|\nabla\phi^{n+1}\|^2 - \|\nabla\phi^n\|^2) + A_2\|\nabla(\phi^{n+1}-\phi^n)\|^2, \tag{3.9}$$

we arrive at

$$-\Big(\nabla\cdot\Big(8\alpha(1-3\alpha)\nabla_p g^{(1)}(\nabla\phi^n) + 16\alpha^2\nabla_p g^{(2)}(\nabla\phi^n)\Big), \phi^{n+1}-\phi^n\Big) \geq \tilde{E}_S(\phi^{n+1}) - \tilde{E}_S(\phi^n) - A_2\|\nabla(\phi^{n+1}-\phi^n)\|^2. \tag{3.10}$$

Therefore, a substitution of (3.4) – (3.6) and (3.10) into (3.3) yields

$$0 \geq \frac{1}{4}(\|\phi^{n+1}\|_{L^4} - \|\phi^n\|_{L^4}) - \frac{1}{2}(\|\phi^{n+1}\|^2 - \|\phi^n\|^2) + \frac{(1-3\alpha)^2\varepsilon^2}{2}(\|\nabla\phi^{n+1}\|^2 - \|\nabla\phi^n\|^2) + \frac{\varepsilon^2}{2}(\tilde{E}_S(\phi^{n+1}) - \tilde{E}_S(\phi^n)) + (\frac{(1-3\alpha)^2}{2} + \tilde{A}_2 - \frac{A_2}{2})\varepsilon^2\|\nabla(\phi^{n+1}-\phi^n)\|^2. \tag{3.11}$$

Based on our choice $\tilde{A}_2 = \frac{1}{2}\max(A_2 - (1-3\alpha)^2, 0)$, we have

$$\frac{(1-3\alpha)^2}{2} + \tilde{A}_2 - \frac{A_2}{2} \geq 0, \tag{3.12}$$

and its substitution into (3.11) results in the desired energy stability inequality:

$$E(\phi^{n+1}) - E(\phi^n) \leq 0. \tag{3.13}$$

This finishes the proof of Theorem 3.1. □

Remark 3.2. We refer to this scheme (3.1) – (3.2) as a weakly nonlinear scheme because only the nonlinearity associated to the double well energy needs to be dealt with implicitly in order to obtain an energy stability result. This is an important point, since most often this term is associated with a positivity property of the equation, and it must be treated implicitly to maintain positivity numerically. See, for example, [15], where the singular Flory-Huggins-type double well potential is treated. For simplicity of presentation, we focus on the polynomial approximation in the double well energy potential, as given by (1.1), in which the positivity-preserving property is not available. Meanwhile, for the anisotropic model with a Flory-Huggins-type double well potential – which would presumably yield a positivity property – the corresponding convexity and energy stability analysis could be carried out in a similar way, and the details are left to future works.

Remark 3.3. The convex splitting framework, poularized by Eyre's pioneering work [29], has been successfully applied to various gradient model, such as the phase field crystal (PFC) equation and the modified version [1,2,27,40,53,57]; epitaxial thin film growth models [11,14,20,52]; non-local gradient model [35–37]; phase field model coupled with fluid flow [12,13, 24,25,31,42,55]; *et cetera*. In this approach, the unique solvability and energy stability could be established via a variational inequality framework.

Meanwhile, we observe that the proposed numerical scheme (3.1) – (3.2) does not come from a direct application of convex splitting. In fact, a standard convex splitting scheme, based on the convex-concave decomposition in (2.29) – (2.30), results in an artificial regularization in the form of $-A_2\varepsilon^2\Delta(\phi^{n+1}-\phi^n)$. In comparison, our proposed scheme contains an artificial regularization in the form of $-\tilde{A}_2\varepsilon^2\Delta(\phi^{n+1}-\phi^n)$, with $\tilde{A}_2 \leq \frac{A_2}{2}$, leading to less numerical dissipation. In addition, in the region of sufficiently small α, $\tilde{A}_2$ could be taken as 0, so that an artificial regularization is not needed; just the constant coefficient surface diffusion part is sufficient to stabilize the numerical scheme.

The key reason for the significant difference is that the convexity of the constant coefficient surface diffusion term, with a given energy density of $\frac{(1-3\alpha)^2}{2}\|\nabla\phi\|^2$, brings more extra stabilization that can be used to reduce the size of A_2. Similar stabilization also exists in the convexity analysis of $H_2(\phi)$. In turn, we make use of the additional stabilization estimates, which in turn lead to a much reduced artificial regularization, while preserving the energy stability.

Remark 3.4. In the physical system (1.1) and (1.3) discussed in this article, the anisotropic interfacial function $\gamma(\boldsymbol{n})$ is only placed in the surface diffusion part, and the double-well potential still keeps the standard type. In more recent works [50, 51], such an interfacial energy function has been placed in both the surface diffusion and double-well potential part. In this updated model, the double-well surface density function may even become negative for sufficiently strong anisotropy. The analysis for this model is more challenging than the one presented in this article, and we will leave this analysis in the

in which a stabilized SAV algorithm is applied to the Allen-Cahn model. Again, such an energy stability is in terms of a numerically modified variable; in comparison, the stability estimate reported in Theorem 3.1 is based on the energy functional in the original phase variable.

Remark 3.6. For simplicity of presentation, we only focus on first-order energy stable schemes for the anisotropic Cahn-Hilliard equation. A second-order energy stable algorithm could be constructed using similar techniques of convexity analysis, combined with the second-order backward differentiation formula (BDF2) for temporal approximation; also see the related works [19,58] for the isotropic model. The details of the second-order schemes will be left to future investigations.

4. Convergence analysis

The following estimate is needed in the convergence analysis; its proof will be provided in Appendix B.

Lemma 4.1. *For any* $\boldsymbol{p}_1, \boldsymbol{p}_2 \in \mathbb{R}^3$,

$$\left|\partial_{p_i} g^{(k)}(\boldsymbol{p}_1) - \partial_{p_i} g^{(k)}(\boldsymbol{p}_2)\right| \le \left(D_1^{(k)} - D_2^{(k)}\right)|\tilde{q}_i| + D_2^{(k)} \sum_{j=1}^{3} |\tilde{q}_i|, \quad k = 1, 2, \quad i = 1, 2, 3, \tag{4.1}$$

where $\tilde{\boldsymbol{q}} := \boldsymbol{p}_2 - \boldsymbol{p}_1$.

We will assume from this point forward that $B_0^{(1)} = \frac{15}{2}$ and $B_0^{(2)} = 12$, so that

$$B_0^{(k)} = D_1^{(k)} + 2D_2^{(k)}.$$

In this section, we look at the region of sufficiently small α, i.e.,

$$\gamma_0 := (1 - 3\alpha)^2 - (8\alpha^2 B_0^{(2)} + 4\alpha|1 - 3\alpha|B_0^{(1)}) > 0. \tag{4.2}$$

In this case $\tilde{A}_2 = 0$. It was proved in the related work [43] that, a global in time weak solution (in the variational form) could be established with an H^2_{per} initial data, if a Willmore regularization is applied. The PDE solution with higher order regularity could also be derived using certain local in time analysis techniques: for any H^m_{per} initial data (with $m \ge 2$), there is a solution with a local-in-time H^m estimate. In addition, the model without Willmore regularization could be analyzed in a similar manner, under a requirement of sufficiently small α, such as (4.2). In this region, the following convergence result is valid assuming that the PDE solution has sufficient regularity.

Theorem 4.2. *Let* Φ *be the exact periodic solution of the anisotropic CH equation* (1.3) *with the initial data* $\Phi(0) = \phi_0 \in H^m_{\text{per}}(\Omega)$, *with m sufficiently large. For the parameter* α *satisfying condition* (4.2), *suppose* ϕ *is the space-continuous numerical solution of* (3.1) – (3.2). *Then the following error estimate is valid:*

$$\|\Phi - \phi\|_{\ell^\infty(0,T;H^{-1}_{\text{per}})} + \|\Phi - \phi\|_{\ell^2(0,T;H^1_{\text{per}})} \le C\Delta t, \tag{4.3}$$

where the constant $C > 0$ *is independent of* Δt *but depends on the regularity of the exact solution, the equation parameters,* ε *and* α, *and the final time T, where it is assumed that* $T = \Delta t \cdot N_T$, *for some positive integer* N_T.

Proof. Define $\Phi^k = \Phi(\cdot, t_k)$. A detailed Taylor expansion implies the following truncation error:

$$\frac{\Phi^{n+1} - \Phi^n}{\Delta t} = \Delta\Big((\Phi^{n+1})^3 - \Phi^n - (1 - 3\alpha)^2\varepsilon^2\Delta\Phi^{n+1} - \tilde{A}_2\varepsilon^2\Delta(\Phi^{n+1} - \Phi^n) - \varepsilon^2\nabla\cdot\Big(4\alpha(1 - 3\alpha)\nabla_p g^{(1)}(\nabla\phi^n) + 8\alpha^2\nabla_p g^{(2)}(\nabla\phi^n)\Big)\Big) + \tau^n, \tag{4.4}$$

with $\|\tau^n\| \le C\Delta t$. Consequently, with an introduction of the error function

$$\begin{aligned}\frac{e^{n+1}-e^n}{\Delta t} = \Delta\Big(\Big((\Phi^{n+1})^2+\Phi^{n+1}\phi^{n+1}+(\phi^{n+1})^2\Big)e^{n+1}-e^n \\ -(1-3\alpha)^2\varepsilon^2\Delta e^{n+1}-\tilde{A}_2\varepsilon^2\Delta(e^{n+1}-e^n) \\ -\varepsilon^2\nabla\cdot\Big(4\alpha(1-3\alpha)\Big(\nabla_p g^{(1)}(\nabla\Phi^n)-\nabla_p g^{(1)}(\nabla\phi^n)\Big) \\ +8\alpha^2\Big(\nabla_p g^{(2)}(\nabla\Phi^n)-\nabla_p g^{(2)}(\nabla\phi^n)\Big)\Big)+\tau^n. \end{aligned} \tag{4.6}$$

Meanwhile, we recall that the exact solution to the CH equation (1.3) is mass conservative:

$$\int_\Omega \Phi(\boldsymbol{x},t)\,d\boldsymbol{x}\equiv\int_\Omega \Phi(\boldsymbol{x},0)\,d\boldsymbol{x},\quad \forall t>0.$$

On the other hand, the numerical solution (3.1)-(3.2) is also mass conservative. In turn, we conclude that the numerical error function $e^k\in\mathring{H}^1_{\rm per}(\Omega)$, that is, it has zero mean:

$$\overline{e^k}:=\frac{1}{|\Omega|}\int_\Omega e^k\,d\boldsymbol{x}=\frac{1}{|\Omega|}\int_\Omega e^0=0,\quad \text{since}\quad e^0\equiv 0. \tag{4.7}$$

Consequently, we define $\psi^k:=(-\Delta)^{-1}e^k\in\mathring{H}^{-1}_{\rm per}(\Omega)$ via

$$-\Delta\psi^k=e^k,\quad \text{where}\quad \int_\Omega \psi^k\,d\boldsymbol{x}=0.$$

Taking the L^2 inner product of the error equation (4.6) with $2\psi^{n+1}$ gives

$$\begin{aligned}&\|e^{n+1}\|^2_{\mathring{H}^{-1}_{\rm per}}-\|e^n\|^2_{\mathring{H}^{-1}_{\rm per}}+\|e^{n+1}-e^n\|^2_{\mathring{H}^{-1}_{\rm per}}+2(1-3\alpha)^2\varepsilon^2\Delta t\|\nabla e^{n+1}\|^2 \\ &-2\tilde{A}_2\varepsilon^2\Delta t\left(\Delta(e^{n+1}-e^n),e^{n+1}\right) \\ &\quad=-2\Delta t\Big(\Big((\Phi^{n+1})^2+\Phi^{n+1}\phi^{n+1}+(\phi^{n+1})^2\Big)e^{n+1},e^{n+1}\Big)+2\Delta t(e^n,e^{n+1})+2\Delta t(\tau^n,\psi^{n+1}) \\ &\qquad-8\alpha(1-3\alpha)\varepsilon^2\Delta t\Big(\nabla_p g^{(1)}(\nabla\Phi^n)-\nabla_p g^{(1)}(\nabla\phi^n),\nabla e^{n+1}\Big) \\ &\qquad-16\alpha^2\varepsilon^2\Delta t\Big(\nabla_p g^{(2)}(\nabla\Phi^n)-\nabla_p g^{(2)}(\nabla\phi^n),\nabla e^{n+1}\Big),\end{aligned} \tag{4.8}$$

where integration-by-parts has been repeatedly applied.

The following inequality is valid for the last term on the left hand side:

$$-\left(\Delta(e^{n+1}-e^n),e^{n+1}\right)=\left(\nabla(e^{n+1}-e^n),\nabla e^{n+1}\right)\ge\frac{1}{2}(\|\nabla e^{n+1}\|^2-\|\nabla e^n\|^2). \tag{4.9}$$

The first term on the right hand side is always non-positive:

$$-\Big(\Big((\Phi^{n+1})^2+\Phi^{n+1}\phi^{n+1}+(\phi^{n+1})^2\Big)e^{n+1},e^{n+1}\Big)\le 0, \tag{4.10}$$

due to the fact that $a^2+ab+b^2\ge 0$ for any $a,b\in\mathbb{R}$. For the concave (expansive) term, the estimate is standard:

$$\begin{aligned}(e^n,e^{n+1})&\le\frac{1}{2}(\|e^n\|^2+\|e^{n+1}\|^2) \\ &\le\frac{\gamma_0\varepsilon^2}{4}(\|\nabla e^n\|^2+\|\nabla e^{n+1}\|^2)+\frac{\varepsilon^{-2}}{4\gamma_0}(\|e^{n+1}\|^2_{\mathring{H}^{-1}_{\rm per}}+\|e^n\|^2_{\mathring{H}^{-1}_{\rm per}}),\end{aligned} \tag{4.11}$$

in which the following interpolation inequality has been applied in the last step:

$$\|e^k\|^2=(\nabla e^k,\nabla(-\Delta)^{-1}e^k)\le\|\nabla e^k\|\cdot\|e^k\|_{\mathring{H}^{-1}}\le\frac{\gamma_0\varepsilon^2}{2}\|\nabla e^k\|^2+\frac{\varepsilon^{-2}}{2\gamma_0}\|e^k\|^2_{\mathring{H}^{-1}}, \tag{4.12}$$

The rest of the proof is focused on the estimates for the nonlinear error terms. We begin with the following expansion

$$-\Big(\nabla_p g^{(k)}(\nabla\Phi^n)-\nabla_p g^{(k)}(\nabla\phi^n),\nabla e^{n+1}\Big)=-\sum_{j=1}^{3}\Big(\partial_{p_j} g^{(k)}(\nabla\Phi^n)-\partial_{p_j} g^{(k)}(\nabla\phi^n),\partial_{x_j} e^{n+1}\Big), \tag{4.14}$$

for $k=1,2$. Applying Lemma 4.1, we get, for $k=1,2$,

$$\begin{aligned}&\Big|\Big(\nabla_p g^{(k)}(\nabla\Phi^n)-\nabla_p g^{(1)}(\nabla\phi^n),\nabla e^{n+1}\Big)\Big|\\&\le\frac{D_1^{(k)}}{2}(\|\nabla e^n\|^2+\|\nabla e^{n+1}\|^2)+D_2^{(k)}(\|\nabla e^n\|^2+\|\nabla e^{n+1}\|^2)\\&=\frac{B_0^{(k)}}{2}(\|\nabla e^n\|^2+\|\nabla e^{n+1}\|^2),\end{aligned} \tag{4.15}$$

due to the fact that $B_0^{(k)}=D_1^{(k)}+2D_2^{(k)}$.

Subsequently, a combination of (4.8), (4.9), (4.10), (4.11), (4.13), and (4.15) yields

$$\begin{aligned}&\|e^{n+1}\|_{\dot H_{\rm per}^{-1}}^2-\|e^n\|_{\dot H_{\rm per}^{-1}}^2+\tilde A_2(\|\nabla e^{n+1}\|^2-\|\nabla e^n\|^2)\\&+\varepsilon^2\Delta t\Big(2(1-3\alpha)^2-4\alpha|1-3\alpha|B_0^{(1)}-8\alpha^2B_0^{(2)}-\frac{\gamma_0}{2}\Big)\|\nabla e^{n+1}\|^2\\&\le\varepsilon^2\Delta t\Big(4\alpha|1-3\alpha|B_0^{(1)}+8\alpha^2B_0^{(2)}+\frac{\gamma_0}{2}\Big)\|\nabla e^n\|^2\\&\quad+\left(\frac{\varepsilon^{-2}}{2\gamma_0}+1\right)\Delta t(\|e^{n+1}\|_{\dot H_{\rm per}^{-1}}^2+\|e^n\|_{\dot H_{\rm per}^{-1}}^2)+\Delta t\|\tau^n\|_{\dot H_{\rm per}^{-1}}^2.\end{aligned} \tag{4.16}$$

Meanwhile, under condition (4.2), we see that

$$\Big(2(1-3\alpha)^2-4\alpha|1-3\alpha|B_0^{(1)}-8\alpha^2B_0^{(2)}-\frac{\gamma_0}{2}\Big)-\Big(4\alpha|1-3\alpha|B_0^{(1)}+8\alpha^2B_0^{(2)}+\frac{\gamma_0}{2}\Big)=\gamma_0>0. \tag{4.17}$$

Summation of (4.16) in time gives

$$\begin{aligned}&\|e^{n+1}\|_{\dot H_{\rm per}^{-1}}^2+\tilde A_2\|\nabla e^{n+1}\|^2+\gamma_0\varepsilon^2\Delta t\sum_{k=0}^{n+1}\|\nabla e^k\|^2\\&\qquad\le\left(\frac{\varepsilon^{-2}}{\gamma_0}+2\right)\Delta t\sum_{k=0}^{n+1}\|e^k\|_{\dot H_{\rm per}^{-1}}^2+\Delta t\sum_{k=0}^{n+1}\|\tau^k\|_{\dot H_{\rm per}^{-1}}^2.\end{aligned} \tag{4.18}$$

Finally, an application of discrete Gronwall inequality leads to an $\ell^\infty(0,T;\dot H_{\rm per}^{-1})\cap\ell^2(0,T;H_{\rm per}^1)$ convergence of the numerical scheme (3.1)-(3.2):

$$\|e^{n+1}\|_{\dot H_{\rm per}^{-1}}^2+\gamma_0\varepsilon^2\Delta t\sum_{k=0}^{n+1}\|\nabla e^k\|^2\le C\Delta t^2, \tag{4.19}$$

for any $1\le n+1\le N_T$, where $T=\Delta t\cdot N_T$. Note that the constant $C>0$ depends on the exact solution, the physical parameters ε and α, and the final time T, but is independent on Δt. The proof of the theorem is completed. □

5. Strong anisotropy and missing orientations

For sufficiently large α, the system is strongly anisotropic, and the associated anisotropic Cahn-Hilliard equation may become ill-posed. Furthermore, the equilibrium shape would have missing orientations without appropriate regularization. With respect to modeling, this is desirable, since crystals with missing orientations are observed in nature. To overcome the difficulty with ill-posedness, a Willmore or biharmonic regularization is usually added. The biharmonic regularization is simpler, and it is may be more preferred [51,54,56] when using the Kobayoshi-type anisotropy model [41]. With such a

and the PDE system becomes

$$\partial_t \phi = \Delta \mu, \quad \mu = \phi^3 - \phi - \varepsilon^2 \nabla \cdot \Big(\gamma^2(\boldsymbol{n}) \nabla \phi + \gamma(\boldsymbol{n}) |\nabla \phi| \mathbf{P} \nabla_n \gamma(\boldsymbol{n}) \Big) + \beta \varepsilon^2 \Delta^2 \phi. \tag{5.2}$$

Since $\int_\Omega (\Delta \phi)^2 d\boldsymbol{x}$ is strictly convex, the convex-concave decomposition for the total energy functional (5.1), with biharmonic regularization, is given by $E(\phi) = E_c(\phi) - E_e(\phi)$, with

$$E_c(\phi) = \int_\Omega \Big(\frac{1}{4}\phi^4 + \frac{1}{4} + \frac{\varepsilon^2}{2}((1-3\alpha)^2 + A_2)|\nabla \phi|^2 + \frac{\beta \varepsilon^2}{2}(\Delta \phi)^2 \Big) d\boldsymbol{x}, \tag{5.3}$$

$$E_e(\phi) = \int_\Omega \Big(\frac{1}{2}\phi^2 + \frac{\varepsilon^2}{2}(-\tilde{E}_S(\phi) + A_2 |\nabla \phi|^2) \Big) d\boldsymbol{x}, \tag{5.4}$$

where both E_c and E_e are convex.

Again, we avoid a direct application of convex splitting. Following similar ideas in the design of the numerical scheme (3.1) – (3.2), we present the following semi-implicit, first-order-in-time numerical scheme:

$$\frac{\phi^{n+1} - \phi^n}{\Delta t} = \Delta \mu(\phi^{n+1}, \phi^n), \tag{5.5}$$

$$\begin{aligned} \mu(\phi^{n+1}, \phi^n) = {} & (\phi^{n+1})^3 - \phi^n - (1-3\alpha)^2 \varepsilon^2 \Delta \phi^{n+1} + \beta \varepsilon^2 \Delta^2 \phi^{n+1} - \tilde{A}_2 \varepsilon^2 \Delta (\phi^{n+1} - \phi^n) \\ & - \varepsilon^2 \nabla \cdot \Big(4\alpha(1-3\alpha) \nabla_p g^{(1)}(\nabla \phi^n) + 8\alpha^2 \nabla_p g^{(2)}(\nabla \phi^n) \Big). \end{aligned} \tag{5.6}$$

The unique solvability and unconditional energy stability could be similarly established as in Theorem 3.1; the details are skipped for the sake of brevity.

Theorem 5.1. *The proposed numerical scheme (5.5) – (5.6) is uniquely solvable and unconditionally energy stable, that is, $E(\phi^{n+1}) \le E(\phi^n)$, for any $\alpha > 0$, provided $B_0^{(1)} = \frac{15}{2}$, $B_0^{(2)} = 12$, and*

$$\tilde{A}_2 = \max\Big(4\alpha^2 B_0^{(2)} + 2\alpha |1-3\alpha| B_0^{(1)} - \frac{1}{2}(1-3\alpha)^2, 0 \Big) = \frac{A_1}{2},$$

where A_1 is given by (2.18).

The convergence result is established in the next theorem, for any $\alpha > 0$, even the for the strongly anisotropic regime. The PDE solution with H^2 regularity has been established in [43], for the Willmore regularization with any $\beta > 0$. The analysis with the biharmonic regularization is expected to be more straightforward. Moreover, higher order H^m estimates would become available with the help of certain local in time analysis techniques.

Theorem 5.2. *Let Φ be the exact periodic solution of the anisotropic CH equation with the biharmonic regularization, with the initial data $\Phi(0) = \phi_0 \in H^m_{\text{per}}(\Omega)$, with m sufficiently large. Suppose that $\alpha \ge 0$ is arbitrary, but $\tilde{A}_2$ is chosen as in the last theorem. Suppose ϕ is the space-continuous numerical solution of (5.5) – (5.6). Then the following error estimate is valid:*

$$\|\Phi - \phi\|_{\ell^\infty(0,T;H^{-1}_{\text{per}})} + \|\Phi - \phi\|_{\ell^2(0,T;H^2_{\text{per}})} \le C \Delta t, \tag{5.7}$$

where the constant $C > 0$ is independent of Δt but depends on the regularity of the exact solution, the equation parameters, ε, α, and β, and the final time T, where it is assumed that $T = \Delta t \cdot N_T$, for some positive integer N_T.

Proof. The proof follows the same idea as the one for Theorem 4.2, with only an addition of the bi-harmonic surface diffusion term. For simplicity of presentation, we use the same notations as in the proof of Theorem 4.2.

A detailed Taylor expansion gives the following truncation error

$$\frac{\Phi^{n+1} - \Phi^n}{\Delta t} = \Lambda \Big((\Phi^{n+1})^3 - \Phi^n - (1-3\alpha)^2 \varepsilon^2 \Lambda \Phi^{n+1} + \beta \varepsilon^2 \Lambda^2 \Phi^{n+1} - \tilde{A}_2 \varepsilon^2 \Lambda (\Phi^{n+1} - \Phi^n)$$

$$\begin{aligned}\frac{e^{n+1}-e^n}{\Delta t} = \Delta\Big(\Big((\Phi^{n+1})^2+\Phi^{n+1}\phi^{n+1}+(\phi^{n+1})^2\Big)e^{n+1}-e^n\\ -(1-3\alpha)^2\varepsilon^2\Delta e^{n+1}+\beta\varepsilon^2\Delta^2 e^{n+1}-\tilde{A}_2\varepsilon^2\Delta(e^{n+1}-e^n)\\ -\varepsilon^2\nabla\cdot\Big(4\alpha(1-3\alpha)\Big(\nabla_p g^{(1)}(\nabla\Phi^n)-\nabla_p g^{(1)}(\nabla\phi^n)\Big)\\ +8\alpha^2\Big(\nabla_p g^{(2)}(\nabla\Phi^n)-\nabla_p g^{(2)}(\nabla\phi^n)\Big)\Big)+\tau^n. \end{aligned} \tag{5.9}$$

In turn, taking an L^2 inner product of the error equation (5.9) with $2\psi^{n+1}$ gives

$$\begin{aligned}&\|e^{n+1}\|^2_{\dot{H}^{-1}_{\rm per}}-\|e^n\|^2_{\dot{H}^{-1}_{\rm per}}+\|e^{n+1}-e^n\|^2_{\dot{H}^{-1}_{\rm per}}+2(1-3\alpha)^2\varepsilon^2\Delta t\|\nabla e^{n+1}\|^2\\ &+2\beta\varepsilon^2\Delta t\|\Delta\phi^{n+1}\|^2-2\tilde{A}_2\varepsilon^2\Delta t\left(\Delta(e^{n+1}-e^n),e^{n+1}\right)\\ &\quad=-2\Delta t\Big(\Big((\Phi^{n+1})^2+\Phi^{n+1}\phi^{n+1}+(\phi^{n+1})^2\Big)e^{n+1},e^{n+1}\Big)+2\Delta t(e^n,e^{n+1})+2\Delta t(\tau^n,\psi^{n+1})\\ &\qquad-8\alpha(1-3\alpha)\varepsilon^2\Delta t\Big(\nabla_p g^{(1)}(\nabla\Phi^n)-\nabla_p g^{(1)}(\nabla\phi^n),\nabla e^{n+1}\Big)\\ &\qquad-16\alpha^2\varepsilon^2\Delta t\Big(\nabla_p g^{(2)}(\nabla\Phi^n)-\nabla_p g^{(2)}(\nabla\phi^n),\nabla e^{n+1}\Big).\end{aligned} \tag{5.10}$$

Estimates (4.9), (4.10), (4.13), and (4.15) are still valid, and inequality (4.11) could be modified as

$$(e^n,e^{n+1})\le\frac{\varepsilon^2}{4}(\|\nabla e^n\|^2+\|\nabla e^{n+1}\|^2)+\frac{\varepsilon^{-2}}{4}(\|e^{n+1}\|^2_{\dot{H}^{-1}_{\rm per}}+\|e^n\|^2_{\dot{H}^{-1}_{\rm per}}). \tag{5.11}$$

A substitution of all these inequalities into (5.10) yields

$$\begin{aligned}&\|e^{n+1}\|^2_{\dot{H}^{-1}_{\rm per}}-\|e^n\|^2_{\dot{H}^{-1}_{\rm per}}+\tilde{A}_2\varepsilon^2(\|\nabla e^{n+1}\|^2-\|\nabla e^n\|^2)+2\beta\varepsilon^2\Delta t\|\Delta\phi^{n+1}\|^2\\ &\quad\le\varepsilon^2\Delta t(\tilde{C}_1\|\nabla e^{n+1}\|^2+\tilde{C}_2\|\nabla e^n\|^2)+\left(\frac{\varepsilon^{-2}}{2}+1\right)\Delta t(\|e^{n+1}\|^2_{\dot{H}^{-1}_{\rm per}}+\|e^n\|^2_{\dot{H}^{-1}_{\rm per}})\\ &\qquad+\Delta t\|\tau^n\|^2_{\dot{H}^{-1}_{\rm per}},\end{aligned} \tag{5.12}$$

where

$$\tilde{C}_1:=\left|2(1-3\alpha)^2-4\alpha|1-3\alpha|B_0^{(1)}-8\alpha^2B_0^{(2)}-\frac{1}{2}\right|$$

and

$$\tilde{C}_2:=4\alpha|1-3\alpha|B_0^{(1)}+8\alpha^2B_0^{(2)}+\frac{1}{2}.$$

Meanwhile, based on the Sobolev interpolation inequality, $\|\nabla f\|\le\|f\|^{1/3}_{\dot{H}^{-1}_{\rm per}}\cdot\|\Delta f\|^{2/3}$, we are able to apply Young's inequality and obtain

$$\tilde{C}_1\|\nabla e^{n+1}\|^2\le\tilde{C}_1\|e^{n+1}\|^{2/3}_{\dot{H}^{-1}_{\rm per}}\cdot\|\Delta e^{n+1}\|^{4/3}\le\frac{\tilde{C}_1^3\beta^{-2}}{3}\|e^{n+1}\|^2_{\dot{H}^{-1}_{\rm per}}+\frac{\beta}{2}\|\Delta e^{n+1}\|^2, \tag{5.13}$$

$$\tilde{C}_2\|\nabla e^{n}\|^2\le\tilde{C}_2\|e^{n}\|^{2/3}_{\dot{H}^{-1}_{\rm per}}\cdot\|\Delta e^{n+1}\|^{4/3}\le\frac{\tilde{C}_2^3\beta^{-2}}{3}\|e^{n}\|^2_{\dot{H}^{-1}_{\rm per}}+\frac{\beta}{2}\|\Delta e^{n}\|^2. \tag{5.14}$$

Going back to (5.12), we arrive at

$$\begin{aligned}&\|e^{n+1}\|^2_{\dot{H}^{-1}_{\rm per}}-\|e^n\|^2_{\dot{H}^{-1}_{\rm per}}+\tilde{A}_2(\|\nabla e^{n+1}\|^2-\|\nabla e^n\|^2)+\frac{3}{2}\beta\varepsilon^2\Delta t\|\Delta\phi^{n+1}\|^2-\frac{1}{2}\beta\varepsilon^2\Delta t\|\Delta\phi^n\|^2\\ &\quad\le\left(\frac{\varepsilon^{-2}}{2}+\frac{(\tilde{C}_1^3+\tilde{C}_2^3)\beta^{-2}\varepsilon^2}{3}+1\right)\Delta t(\|e^{n+1}\|^2_{\dot{H}^{-1}_{\rm per}}+\|e^n\|^2_{\dot{H}^{-1}_{\rm per}})+\Delta t\|\tau^n\|^2_{\dot{H}^{-1}_{\rm per}}.\end{aligned} \tag{5.15}$$

Consequently, an application of discrete Gronwall inequality leads to the desired convergence estimate of the numerical scheme (5.5)-(5.6), in the $\ell^\infty(0,T;\dot{H}^{-1}_{\rm per})\cap\ell^2(0,T;H^2_{\rm per})$ norm:

Remark 5.3. Utilizing the test function $(-\Delta)^{-1}e^{n+1}$, an $\ell^\infty(0,T;\mathring{H}^{-1}_{\rm per})\cap\ell^2(0,T;H^1_{\rm per})$ error estimate is reported in Theorem 4.2. For the anisotropic model with bi-harmonic regularization, the convergence has been improved to an $\ell^\infty(0,T;\mathring{H}^{-1}_{\rm per})\cap\ell^2(0,T;H^2_{\rm per})$ error estimate, due to the bi-harmonic surface diffusion. Moreover, with an alternate test function given by e^{n+1}, an $\ell^\infty(0,T;\ell^2)\cap\ell^2(0,T;H^2_{\rm per})$ error estimate for the proposed numerical scheme, as well as an $\ell^\infty(0,T;\ell^2)\cap\ell^2(0,T;H^3_{\rm per})$ error estimate for the model with bi-harmonic regularization, is expected. However, the nonlinear error estimates have to be performed in a much more delicate way, and the details are left to future works.

6. A fully discrete scheme

6.1. Fourier pseudo-spectral approximation

The Fourier pseudo-spectral method, also referred as the Fourier collocation spectral method, is closely related to the Fourier spectral Galerkin method. However, different from the latter setting, a function can be represented on a grid, which, in turn, simplifies the evaluation of certain operators, and can considerably speed up the calculation when using fast algorithms such as the fast Fourier transform (FFT). See, for example, the descriptions in [3,8,18,21,22,32–34,39].

For simplify of presentation, we assume that the domain is given by $\Omega=(0,1)^3$, $N_x=N_y=N_z=:N\in\mathbb{N}$ and $N\cdot h=1$. We further assume that N is odd: $N=2K+1$, for some $K\in\mathbb{N}$. The analyses for more general cases are a bit more tedious, but can be carried out without essential difficulty. The spatial variables are evaluated on the standard 3D numerical grid Ω_N, which is defined by grid points (x_i,y_j,z_k), with $x_i=ih$, $y_j=jh$, $z_k=kh$, $0\le i,j,k\le 2K+1$. This description for three-dimensional mesh ($d=3$) can be trivially modified for the two-dimensional case ($d=2$). In addition, the grid function space is defined as

$$\mathcal{G}_N:=\left\{f:\mathbb{Z}^3\to\mathbb{R}\;\middle|\; f\text{ is }\Omega_N\text{-periodic}\right\}. \tag{6.1}$$

Given any periodic grid functions $f,g\in\mathcal{G}_N$, the ℓ^2 inner product and norm are defined as

$$\langle f,g\rangle:=h^3\sum_{i,j,k=0}^{N-1}f_{i,j,k}\cdot g_{i,j,k},\quad \|f\|_2:=\sqrt{\langle f,f\rangle}. \tag{6.2}$$

The zero-mean grid function subspace is denoted $\mathring{\mathcal{G}}_N:=\left\{f\in\mathcal{G}_N\;\middle|\;\langle f,1\rangle=:\overline{f}=0\right\}$. For $f\in\mathcal{G}_N$, we have the discrete Fourier expansion

$$f_{i,j,k}=\sum_{\ell,m,n=-K}^{K}\hat{f}^N_{\ell,m,n}\exp\left(2\pi\mathrm{i}(\ell x_i+my_j+nz_k)\right), \tag{6.3}$$

in which the discrete Fourier coefficients are given by

$$\hat{f}^N_{\ell,m,n}:=h^3\sum_{i,j,k=0}^{N-1}f_{i,j,k}\exp\left(-2\pi\mathrm{i}\left(\ell x_i+mx_j+nx_k\right)\right). \tag{6.4}$$

The collocation Fourier spectral first and second order *derivatives* of f are defined as

$$\mathcal{D}_x f_{i,j,k}:=\sum_{\ell,m,n=-K}^{K}(2\pi\mathrm{i}\ell)\,\hat{f}^N_{\ell,m,n}\exp\left(2\pi\mathrm{i}(\ell x_i+my_j+nz_k)\right), \tag{6.5}$$

$$\mathcal{D}_x^2 f_{i,j,k}:=\sum_{\ell,m,n=-K}^{K}\left(-4\pi^2\ell^2\right)\hat{f}^N_{\ell,m,n}\exp\left(2\pi\mathrm{i}(\ell x_i+my_j+nz_k)\right). \tag{6.6}$$

The differentiation operators in the y and z directions, $\mathcal{D}_y$, $\mathcal{D}_y^2$, $\mathcal{D}_z$ and $\mathcal{D}_z^2$ can be defined in the same fashion. In turn, the discrete Laplacian, gradient and divergence operators are given by

$$\Delta_N f:=\left(\mathcal{D}_x^2+\mathcal{D}_y^2+\mathcal{D}_z^2\right)f,\quad \nabla_N f:=\begin{pmatrix}\mathcal{D}_x f\\ \mathcal{D}_y f\end{pmatrix},\quad \nabla_N\cdot\begin{pmatrix}f_1\\ f_2\end{pmatrix}:=\mathcal{D}_x f_1+\mathcal{D}_y f_2+\mathcal{D}_z f_3, \tag{6.7}$$

In addition, the following summation-by-parts formulas are valid (see the related discussions in [11,14,33,34]): for any periodic grid functions $f, g \in \mathcal{G}_N$,

$$\langle f, \Delta_N g \rangle = -\langle \nabla_N f, \nabla_N g \rangle, \quad \left\langle f, \Delta_N^2 g \right\rangle = \langle \Delta_N f, \Delta_N g \rangle. \tag{6.9}$$

Definition 6.1. Suppose that the grid function $f \in \mathcal{G}_N$ has the discrete Fourier expansion (6.3). Its spectral extension into the trigonometric polynomial space $\mathcal{P}_K$ (the space of trigonometric polynomials of degree at most K) is defined as

$$f_S(x, y, z) = \sum_{\ell,m,n=-K}^{K} \hat{f}^N_{\ell,m,n} \exp\left(2\pi \mathrm{i}(\ell x + m y + n z)\right). \tag{6.10}$$

We write $S_N(f) = f_S$ and call $S_N : \mathcal{G}_N \to \mathcal{P}_K$ the spectral interpolation operator. Suppose $g \in C_{\text{per}}(\Omega, \mathbb{R})$. We define the grid projection $Q_N : C_{\text{per}}(\Omega, \mathbb{R}) \to \mathcal{G}_N$ via

$$Q_N(g)_{i,j,k} := g(x_i, y_j, z_k). \tag{6.11}$$

The resultant grid function may, of course, be expressed as a discrete Fourier expansion:

$$Q_N(g)_{i,j,k} = \sum_{\ell,m,n=-K}^{K} \widehat{Q_N(g)}^N_{\ell,m,n} \exp\left(2\pi \mathrm{i}(\ell x_i + m y_j + n z_k)\right).$$

We define the de-aliasing operator $R_N : C_{\text{per}}(\Omega, \mathbb{R}) \to \mathcal{P}_K$ via $R_N := S_N(Q_N)$. In other words,

$$R_N(g)(x, y, z) = \sum_{\ell,m,n=-K}^{K} \widehat{Q_N(g)}^N_{\ell,m,n} \exp\left(2\pi \mathrm{i}(\ell x + m y + n z)\right). \tag{6.12}$$

Finally, for any $g \in L^2(\Omega, \mathbb{R})$, we define the (standard) Fourier projection operator $P_N : L^2(\Omega, \mathbb{R}) \to \mathcal{P}_K$ via

$$P_N(g)(x, y, z) = \sum_{\ell,m,n=-K}^{K} \hat{g}_{\ell,m,n} \exp\left(2\pi \mathrm{i}(\ell x + m y + n z)\right),$$

where

$$\hat{g}_{\ell,m,n} = \int_{\Omega} g(x, y, z) \exp\left(-2\pi \mathrm{i}\,(\ell x + m y + n z)\right) d\boldsymbol{x},$$

are the (standard) Fourier coefficients.

Remark 6.2. Note that, in general, for $g \in C_{\text{per}}(\Omega, \mathbb{R})$, $P_N(g) \neq R_N(g)$, and, in particular,

$$\hat{g}_{\ell,m,n} \neq \widehat{Q_N(g)}^N_{\ell,m,n}.$$

However, if $g \in \mathcal{P}_K$ to begin with, then $\hat{g}_{\ell,m,n} = \widehat{Q_N(g)}^N_{\ell,m,n}$. In other words, $R_N : \mathcal{P}_K \to \mathcal{P}_K$ is the identity operator.

To overcome a key difficulty associated with the H^m bound of the nonlinear term obtained by collocation interpolation, the following lemma is introduced.

Lemma 6.3. *Suppose that m and K are non-negative integers, and, as before, assume that $N = 2K + 1$. For any $\varphi \in \mathcal{P}_{mK}$ in $\mathbb{R}^d$, we have the estimate*

$$\|R_N(\varphi)\|_{H^r} \leq m^{\frac{d}{2}} \|\varphi\|_{H^r}, \tag{6.13}$$

for any non-negative integer r.

See the recent article by Gottlieb and Wang [34] for a proof of the last result. The proof of the following estimate can be found in [8]

We also note the following identity:

Proposition 6.5. *Suppose that $\phi \in C_{\text{per}}(\Omega)$. Then*

$$\mathcal{D}_x Q_N(\phi) = Q_N(\partial_x R_N(\phi)). \tag{6.15}$$

Similar identities are available to the higher order derivatives.

In addition, we introduce the discrete fractional operator $(-\Delta_N)^\gamma$ (with $\gamma > 0$):

$$(-\Delta_N)^\gamma f_{i,j,k} := \sum_{\ell,m,n=-K}^{K} \left(4\pi^2(\ell^2+m^2+n^2)\right)^\gamma \hat{f}^N_{\ell,m,n} \exp\left(2\pi \mathrm{i}(\ell x_i + m y_j + n z_k)\right), \tag{6.16}$$

for a grid function f with the discrete Fourier expansion as (6.3). Similarly, for a grid function $f \in \mathring{\mathcal{G}}_N$ of (discrete) mean zero, a discrete version of the operator $(-\Delta)^{-\gamma}$ may be defined as

$$(-\Delta_N)^{-\gamma} f_{i,j,k} := \sum_{\substack{\ell,m,n=-K \\ (\ell,m,n)\neq \mathbf{0}}}^{K} \left(4\pi^2(\ell^2+m^2+n^2)\right)^{-\gamma} \hat{f}^N_{\ell,m,n} \exp\left(2\pi \mathrm{i}(\ell x_i + m y_j + n z_k)\right). \tag{6.17}$$

Observe that, in this way of defining the inverse operator, the result is a periodic grid function of zero mean, i.e., $(-\Delta_N)^{-\gamma} f \in \mathring{\mathcal{G}}_N$.

Detailed calculations show that the following summation-by-parts formulas are valid (see the related discussions in [11, 14,33,34]): for any periodic grid functions $f, g \in \mathcal{G}_N$,

$$\langle f, \Delta_N g\rangle = -\langle \nabla_N f, \nabla_N g\rangle, \quad \left\langle f, \Delta_N^2 g\right\rangle = \langle \Delta_N f, \Delta_N g\rangle, \quad \left\langle f, \Delta_N^3 g\right\rangle = -\langle \nabla_N \Delta_N f, \nabla_N \Delta_N g\rangle. \tag{6.18}$$

We need a discrete version of the norm $\|\cdot\|_{H^{-1}}$ defined on $\mathring{\mathcal{G}}_N$. For any $f, g \in \mathring{\mathcal{G}}_N$, we define

$$\langle f, g\rangle_{-1,N} := \left\langle f, (-\Delta_N)^{-1} g\right\rangle = \left\langle (-\Delta_N)^{-\frac{1}{2}} f, (-\Delta_N)^{-\frac{1}{2}} g\right\rangle, \tag{6.19}$$

so that the $\|\cdot\|_{-1,N}$ norm could be introduced as

$$\|f\|_{-1,N} := \sqrt{\langle f, f\rangle_{-1,N}} = \|(-\Delta_N)^{-\frac{1}{2}} f\|_2. \tag{6.20}$$

In addition to the standard ℓ^2 norm, we also introduce the ℓ^p, $1 \le p < \infty$, and ℓ^∞ norms for a grid function $f \in \mathcal{G}_N$:

$$\|f\|_\infty := \max_{i,j,k} |f_{i,j,k}|, \qquad \|f\|_p := \left(h^3 \sum_{i,j,k=0}^{N-1} |f_{i,j,k}|^p\right)^{\frac{1}{p}}, \quad 1 \le p < \infty. \tag{6.21}$$

The discrete H^1 and H^2 norms are introduced as

$$\|f\|^2_{H^1_N} = \|f\|_2^2 + \|\nabla_N f\|_2^2, \quad \|f\|^2_{H^2_N} = \|f\|^2_{H^1_N} + \|\Delta_N f\|_2^2. \tag{6.22}$$

For any $\phi \in \mathcal{G}_N$, the discrete energy for the regularized system (5.1) is defined as

$$E_N(\phi) := \frac{1}{4}\|\phi\|_4^4 - \frac{1}{2}\|\phi\|_2^2 + \frac{1}{4}|\Omega| + E_{S,N}(\phi) + \frac{\beta\varepsilon^2}{2}\|\Delta_N \phi\|_2^2, \tag{6.23}$$

where

$$E_{S,N}(\phi) := (1-3\alpha)^2 \|\nabla_N \phi\|_2 + 8\alpha(1-3\alpha)\langle g^{(1)}(\nabla_N \phi), \mathbf{1}\rangle + 16\alpha^2 \langle g^{(2)}(\nabla_N \phi), \mathbf{1}\rangle. \tag{6.24}$$

6.2. The fully discrete scheme and theoretical results

For simplicity of presentation, we focus on the strongly anisotropic Cahn-Hilliard system (5.1), in which a biharmonic

$$\frac{\phi^{n+1}-\phi^n}{\Delta t} = \Delta_N \mu_N(\phi^{n+1},\phi^n), \tag{6.25}$$

$$\mu_N(\phi^{n+1},\phi^n) = (\phi^{n+1})^3 - \phi^n - (1-3\alpha)^2\varepsilon^2\Delta_N\phi^{n+1} + \beta\varepsilon^2\Delta_N^2\phi^{n+1} - \tilde{A}_2\varepsilon^2\Delta_N(\phi^{n+1}-\phi^n)$$
$$-\varepsilon^2\nabla_N\cdot\Big(4\alpha(1-3\alpha)\nabla_p g^{(1)}(\nabla_N\phi^n) + 8\alpha^2\nabla_p g^{(2)}(\nabla_N\phi^n)\Big). \tag{6.26}$$

The unique solvability and unconditional energy stability estimates follow similar ideas as in the analysis presented in Theorems 3.1, 5.1. In particular, the summation by parts formulas (6.18) have greatly helped the fully discrete analysis. The technical details are left for interested readers.

Theorem 6.6. *The proposed numerical scheme (6.25)-(6.26) is uniquely solvable and unconditionally energy stable:* $E_N(\phi^{n+1}) \le E_N(\phi^n)$.

Before the statement of the convergence analysis for the fully discrete scheme, we define $\Phi_N(\cdot,t) := \mathcal{P}_N\Phi_1(\cdot,t)$ as the (spatial) Fourier projection of the exact solution into $\mathcal{B}^K$, the space of trigonometric polynomials of degree to and including K (with $N = 2K+1$). The initial data for the numerical scheme (6.25)-(6.26) is taken as the point-wise interpolation of Φ_N at $t=0$; $\phi^0 = \mathcal{P}_h\Phi_N(\cdot,t=0)$, i.e., $\phi^0_{i,j,k} := \Phi_N(x_i,y_j,z_k,t=0)$. In turn, the $\|\cdot\|_{-1,N}$ norm is well defined for the error function between the numerical solution ϕ^n and the exact projection solution Φ_N.

The convergence result is available for any $\alpha > 0$; the technical details are left for interested readers. With initial data with sufficient regularity, we could assume that the exact solution has regularity of class $\mathcal{R}$:

$$\Phi \in \mathcal{R} := H^2\left(0,T;C_{\text{per}}(\Omega)\right) \cap H^1\left(0,T;C^6_{\text{per}}(\Omega)\right) \cap L^\infty\left(0,T;H^{m+6}_{\text{per}}(\Omega)\right). \tag{6.27}$$

Theorem 6.7. *Let Φ be the exact periodic solution with of the anisotropic CH equation with the bi-harmonic regularization, with the initial data $\Phi(0) = \phi_0 \in H^{m+6}_{\text{per}}(\Omega)$, and with the regularity class $\mathcal{R}$ given by (6.27). For any $\alpha > 0$, suppose ϕ is the fully discrete numerical solution of (6.25) – (6.26). Then the following error estimate is valid:*

$$\|\Phi_N^n - \phi^n\|_{-1,N} + \left(\beta\varepsilon^2\Delta t\sum_{k=0}^{n}\|\nabla_N(\Phi_N-\phi)\|_2^2\right)^{1/2} \le C(\Delta t + h^m), \tag{6.28}$$

where the constant $C > 0$ is independent of Δt and h but depends on the regularity of the exact solution.

7. Numerical results

7.1. Convergence test for the numerical scheme

In this subsection we perform some numerical tests to verify the accuracy order of the proposed numerical scheme (6.25)-(6.26), including the one with $\beta = 0$ for $\alpha = 0.02$ (so that (4.2) is satisfied), and the one with biharmonic regularization coefficient $\beta = 1$, for an increasing value $\alpha = 0.2$. The explicit treatment for the nonlinear singular parts $g^{(1)}$ and $g^{(2)}$ in the surface diffusion part has greatly improved the numerical efficiency; only a weakly nonlinear term, ϕ^3, needs to be handled at each time step. In this work, we make use of a preconditioned steepest descent (PSD) solver [30] to implement the proposed numerical schemes. Such a solver turns out to be highly efficient, because of its weakly nonlinear nature; the search direction and Poisson-like equations can be solved by using the FFT-based algorithms.

To test the convergence rate, we choose the following exact solution for (1.3) on the square domain $\Omega = (0,1)^2$:

$$\phi_e(x,y,t) = \frac{1}{2\pi}\sin(2\pi x)\cos(2\pi y)\cos(t). \tag{7.1}$$

The physical parameters are set as $\varepsilon = 0.5$, $\alpha = 0.02$, and we choose the artificial diffusion coefficient given by $\tilde{A}_2 = \max\left(4\alpha^2 B_0^{(2)} + 2\alpha|1-3\alpha|B_0^{(1)} - \frac{1}{2}(1-3\alpha)^2, 0\right) = \frac{A_1}{2}$. The final time is taken as $T = 1$.

Due to the spectral accuracy in space, we focus on the convergence test for the temporal numerical error. In turn, we fix the spatial resolution as $N = 256$ so that the numerical error is dominated by the temporal ones. We compute solutions with a sequence of time step sizes, $\Delta t = \frac{T}{N_T}$, with $N_T = 100$ to $N_T = 800$ in increments of 100, and the same final time $T = 1$. The left part of Fig. 1 shows the discrete ℓ^2 norms of the errors between the numerical solution (6.25)-(6.26) (with $\beta = 0$) and exact solution (1.3) (with force terms). To obtain a precise accuracy order, we also present the least square approximation to the GN^{-1} curve, displayed as the straight line in the figure. A careful calculation reveals the slope as

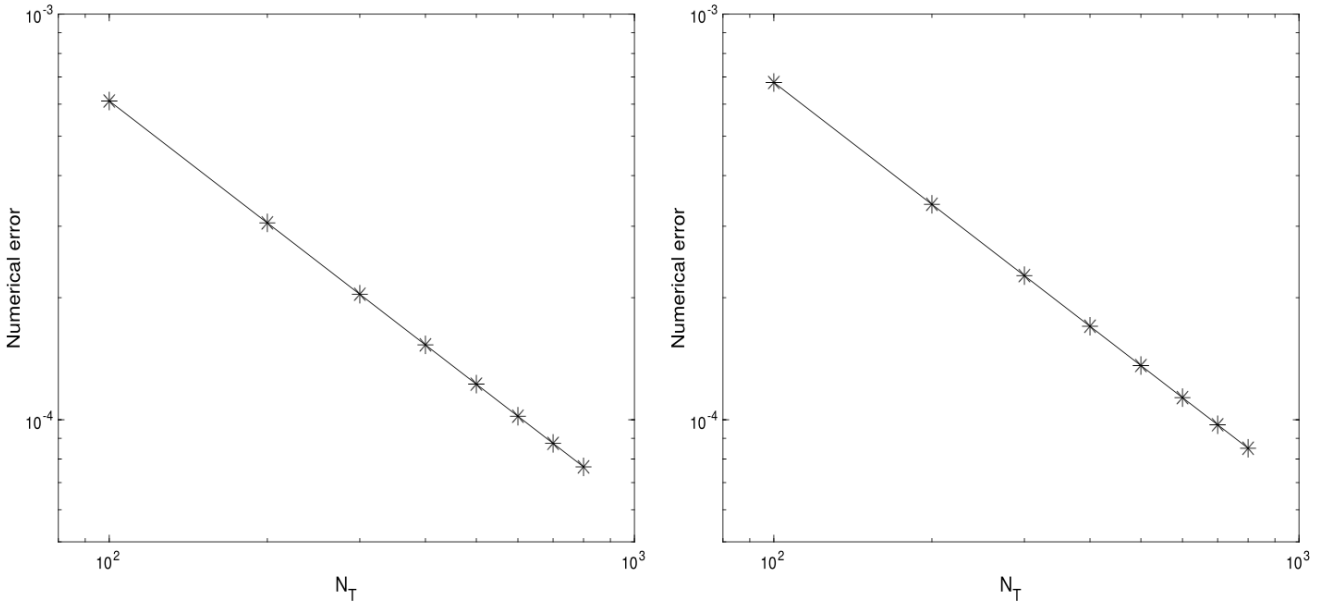

Fig. 1. Left: Discrete ℓ^2 numerical errors for the phase variable at $T = 1$, plotted versus N_T, the number of time steps, for the numerical scheme (6.25)-(6.26) with $\beta = 0$, $\alpha = 0.02$. Right: The corresponding numerical errors for the fully discrete numerical scheme (6.25)-(6.26), with $\beta = 1$, $\alpha = 0.2$. The spatial resolution is fixed as $N = 256$. The star line represents the numerical error plot versus N_T, while the straight line is the least square approximation to the CN_T^{-1} curve. The least square slope is calculated as -0.9989 -0.9987, respectively. These constants have confirmed the first-order temporal accuracy of the proposed scheme.

the temporal accuracy, and the solutions with a sequence of time step sizes: $\Delta t = \frac{T}{N_T}$ (with $N_T = 100$ to $N_T = 800$), are computed with the same final time $T = 1$. The right part of Fig. 1 shows The discrete ℓ^2 norms of the errors between the numerical solution (6.25)-(6.26) (with $\beta = 1$) and exact solution (5.2). Similarly, we display the least square approximation to the CN_T^{-1} curve as the straight line, and the numerical evidence reveals the slope as -0.9986. Again, an obvious first order accuracy is verified.

In the numerical convergence test, an order $O(1)$ value of β is chosen for the biharmonic regularization coefficient, which leads to a perfect accuracy order. For a smaller value of β, the convergence test becomes available only in a shorter time interval, since the convergence constants presented in the estimate (6.28) is of the form of $\exp(CT\beta^{-1}\varepsilon^{-2})$. As the time scale passes through $O(\beta\varepsilon^2)$, the convergence estimate for a fixed time instant may not be observable, while the numerical stability still persists. Meanwhile, extensive numerical simulation results have demonstrated the long time average agreement with certain physical laws for various gradient flows in the large time scale computations with smaller values of β and ε, provided that the numerical method is energy stable; see the related works for the no-slope-selection thin film growth model [11,14,20], etc. These numerical experiments have in turn demonstrated the importance of energy stability of the algorithm, since it is a uniform-in-time property.

7.2. Numerical simulation of anisotropic flow with biharmonic regularization

We perform numerical simulation for the anisotropic Cahn-Hilliard system (5.2) with the biharmonic regularization. The physical parameters are chosen as: $\Omega = (0, 3.2)^2$, $\varepsilon = 0.03$, $\alpha = 0.2$, and initial data for the simulation are set as

$$\phi(x, y, t = 0) = -\tanh\Big(\frac{(x - x_0)^2 + (y - y_0)^2 - r_0}{0.25\varepsilon}\Big), \quad \text{with } x_0 = y_0 = 1.6, r_0 = 0.8. \tag{7.2}$$

The biharmonic regularization coefficient is set as $\beta = 0.0005$, and we take the temporal step size as $\Delta t = 10^{-3}$. The time snapshots of the evolution computed by the proposed numerical scheme (6.25)-(6.26), with spatial resolution 512^2, are presented in Figs. 2. These results demonstrate the combined effects of anisotropy and coarsening; the circular profile evolves to an anisotropic shape with missing orientation at the four corners.

7.3. Impact of the biharmonic regularization parameter

The impact of the biharmonic regularization parameter β has attracted a great deal of attentions in recent years. In

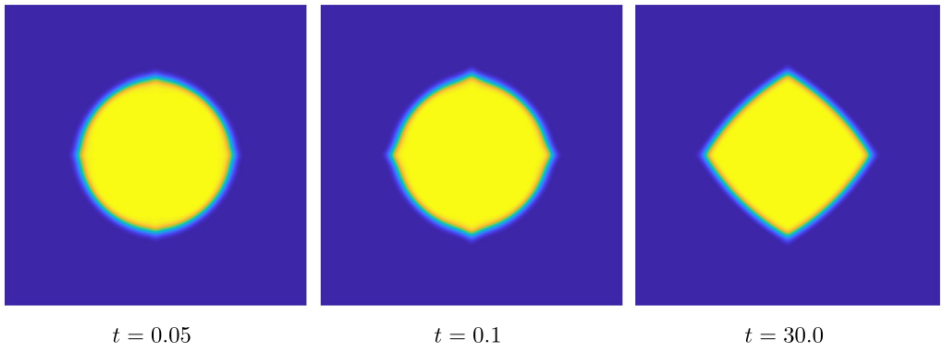

Fig. 2. Time snapshots of the evolution for the anisotropic Cahn-Hilliard model, with $\alpha = 0.2$ and biharmonic regularization coefficient $\beta = 0.0005$. The time sequence for the snapshots is set as $t = 0.05$, 0.1, and 30. The parameters are $\varepsilon = 0.03, \Omega = (0, 3.2)^2$.

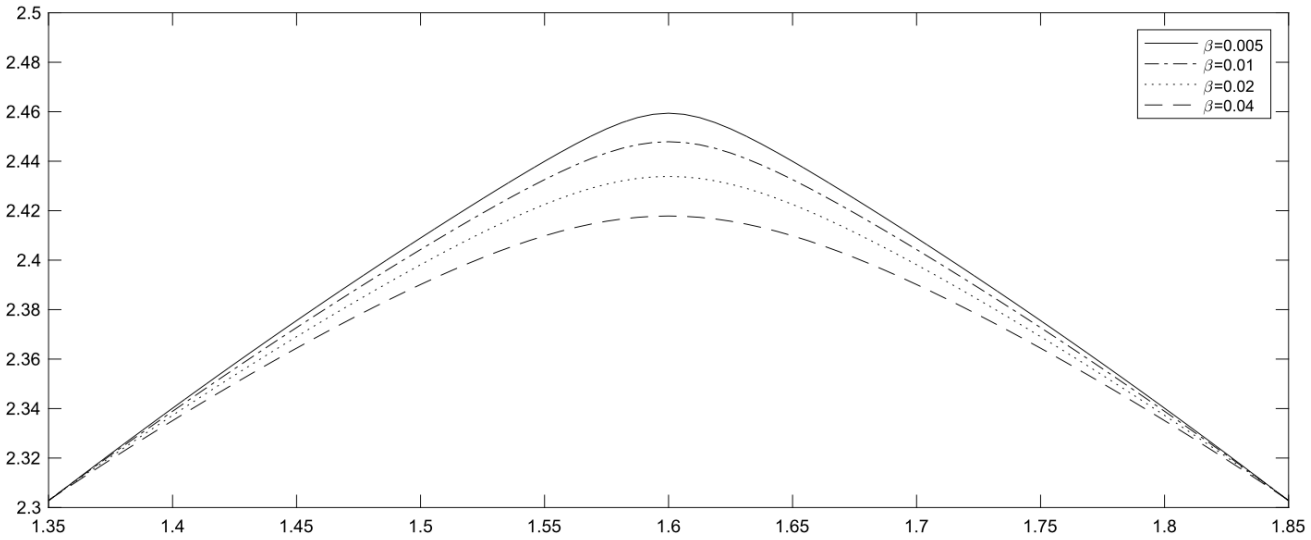

Fig. 3. Comparison of the $\phi = 0.0$ iso-contour plots for numerical solutions obtained with four different corner regularization parameters, $\beta = 0.004$, 0.002, 0.001 and 0.0005, at $t = 30$. The initial data is given by (7.2), and the other physical parameters are set as $\varepsilon = 0.03, \Omega = (0, 3.2)^2$. As the regularization parameter is decreased, the equilibrium $\phi = 0$ iso-contour approaches the Wulff shape, which in this case of strong anisotropy has missing orientations. In particular, a sharp corner would appear in the Wulff shape at $x = 1.6$ [56].

patterns are similar, while smaller regularization coefficient leads to less numerical smearing and sharper profile around the corner area.

7.4. Simulation results using an eight-fold symmetric anisotropic function

As one more example, we present the dynamics of the initial value (7.2) using an eight-fold symmetric anisotropic function [16,17,45,48]

$$\gamma(\boldsymbol{n}) = 1 + \alpha\Big(8\sum_{i=1}^{d}(8n_i^8 - 10n_i^6 + n_i^4) + 9\Big). \tag{7.3}$$

The physical parameters are set as: $\varepsilon = 0.03$, $\alpha = 0.2$, $\beta = 0.002$, $\Delta t = 10^{-4}$. The time snapshots of the evolution computed by the proposed numerical scheme (6.25) – (6.26), with spatial resolution 512^2, are presented in Figs. 4. An octagonal shape has been clearly observed.

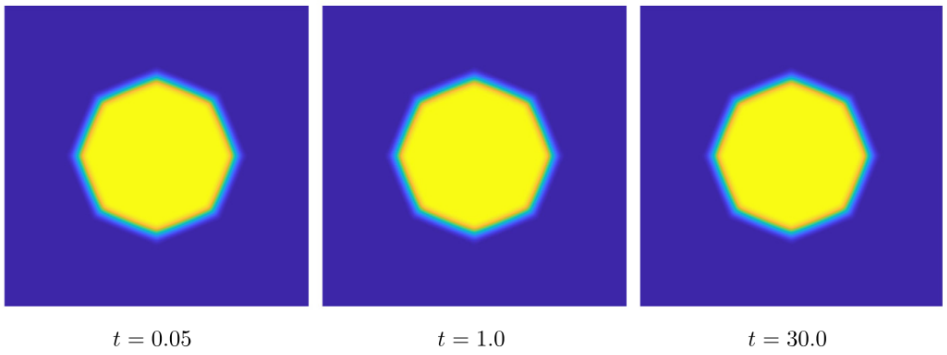

Fig. 4. Time snapshots of the evolution for the anisotropic Cahn-Hilliard model, with an eight-fold symmetric anisotropic function (7.3). The time sequence for the snapshots is set as $t = 0.05, 1, 5$ and 30. The parameters are $\varepsilon = 0.03$, $\alpha = 0.2$, $\Omega = (0, 3.2)^2$.

Fig. 5. The evolutionary surface plots of $\phi = 0$ for the 3-D anisotropic Cahn-Hilliard model, with a four-fold symmetric anisotropic function and initial data (7.4). The time sequence for the snapshots is set as $t = 0.05, 0.1, 1$ and 10. The parameters are $\varepsilon = 0.03$, $\alpha = 0.2$, $\Omega = (0, 3.2)^3$.

7.5. Three-dimensional simulation results

Finally, we present three-dimensional (3-D) numerical simulation results using the four-fold anisotropic function (1.1). The initial data are given by

$$\phi(x, y, z, t = 0) = -\tanh\Big(\frac{(x - x_0)^2 + (y - y_0)^2 + (z - z_0)^2 - r_0}{0.25\varepsilon}\Big), \tag{7.4}$$

with $x_0 = y_0 = z_0 = 1.6$, $r_0 = 0.8$. The physical parameters are set as: $\varepsilon = 0.03$, $\alpha = 0.2$, $\beta = 0.0005$, $\Delta t = 10^{-3}$. The evolutionary surface plots of $\phi = 0$ for the numerical solution computed by the proposed numerical scheme (6.25) – (6.26), with spatial resolution 192^3, are presented in Figs. 5.

8. Concluding remarks

In this article, we propose and analyze an energy stable numerical scheme for the strongly anisotropic Cahn-Hilliard model. To overcome a well-known difficulty associated with the highly nonlinear and singular nature of the anisotropic surface energy, we perform a convexity analysis to the surface energy potential. In more details, a careful estimate reveals that all its second order functional derivatives are uniformly bounded by a global constant. Because of this fact, we are able to treat the nonlinear surface energy part by an explicit method, while preserving the energy stability, via an approach of Doulas-Dupont type regularization. Such an explicit treatment greatly improves the computational efficiency. In addition, its combination with a semi-implicit, energy stable approximation to the double-well potential part leads to a weakly nonlinear numerical scheme. Furthermore, such an energy stability is in terms of the energy potential in the original phase variable, and no auxiliary variable needs to be introduced. With a careful application of the global bound for the second order functional derivatives, an optimal rate convergence analysis becomes available for the proposed numerical scheme, which is the first such result in this area. For a Cahn-Hilliard system with increasing anisotropic parameter α, a biharmonic regularization is introduced to make the equation well-posed, and the proposed numerical scheme turns out to be uniquely solvable, energy stable and convergent. The Fourier pseudo-spectral spatial approximation is chosen as the spatial discretization, and all the theoretical results has been extended for the fully discrete scheme. A few numerical results have also been presented in this work, including the convergence test, simulation results of strongly anisotropic system, numerical investigation of the impact of the biharmonic regularization parameters, etc.

Acknowledgements

This work is supported in part by the Longshan Talent Project of SWUST (PRC) 18LZX529 (K. Cheng), the National Science Foundation (USA) grants NSF DMS-1418689 (C. Wang), and NSF DMS-1719854 (S. Wise).

Appendix A. Proof of Lemma 2.1

For simplicity of presentation, we set $x = x_1,\ y = x_2,\ z = x_3$. First, we recall the expansion formulas for $(x^2+y^2+z^2)^k$, with $2 \le k \le 5$:

$$(x^2+y^2+z^2)^2 = x^4+y^4+z^4+2(x^2y^2+x^2z^2+y^2z^2), \tag{A.1}$$

$$(x^2+y^2+z^2)^3 = x^6+y^6+z^6+3(x^4y^2+x^4z^2+x^2y^4+x^2z^4+y^4z^2+y^2z^4)+6x^2y^2z^2, \tag{A.2}$$

$$\begin{aligned}(x^2+y^2+z^2)^4 = {}& x^8+y^8+z^8+4(x^6y^2+x^6z^2+x^2y^6+x^2z^6+y^6z^2+y^2z^6)\\ & +6(x^4y^4+x^4z^4+y^4z^4)+12(x^4y^2z^2+x^2y^4z^2+x^2y^2z^4),\end{aligned} \tag{A.3}$$

$$\begin{aligned}(x^2+y^2+z^2)^5 = {}& x^{10}+y^{10}+z^{10}+5(x^8y^2+x^8z^2+x^2y^8+x^2z^8+y^8z^2+y^2z^8)\\ & +10(x^6y^4+x^6z^4+x^4y^6+x^4z^6+y^6z^4+y^4z^6)\\ & +20(x^6y^2z^2+x^2y^6z^2+x^2y^2z^6)+30(x^4y^4z^2+x^4y^2z^4+x^2y^4z^4).\end{aligned} \tag{A.4}$$

In addition, the following preliminary estimates are needed in the proof of the two lemmas.

Lemma A.1. *Let $\boldsymbol{x} = (x, y, z) \in \mathbb{R}^3$, and define the following polynomials:*

$$f_1(\boldsymbol{x}) = 8xy(-2x^2y^2-y^2z^2-x^2z^2+z^4), \tag{A.5}$$

$$f_2(\boldsymbol{x}) = 2x^6-2y^6-2z^6+6x^4(y^2+z^2)+18x^2(y^4+z^4)+24x^2y^2z^2-2(y^4z^2+y^2z^4), \tag{A.6}$$

$$f_3(\boldsymbol{x}) = 8xy(3y^4+6z^4-6x^2z^2-3y^2z^2-9x^2y^2), \tag{A.7}$$

$$f_4(\boldsymbol{x}) = 8xy^3(x^4+4x^2y^2+4x^2z^2-3y^4-3z^4), \tag{A.8}$$

$$f_5(\boldsymbol{x}) = -6x^6-6y^6-6z^6-30x^4(y^2+z^2)+66x^2(y^4+z^4)+48x^2y^2z^2-6(y^4z^2+y^2z^4), \tag{A.9}$$

$$f_6(\boldsymbol{x}) = 8x^4(x^4+4x^2y^2+4x^2z^2-3y^4-3z^4), \tag{A.10}$$

$$\begin{aligned}f_7(\boldsymbol{x}) &= f_3(\boldsymbol{x})(x^4+y^4+z^4)+f_4(\boldsymbol{x})(x^2+y^2+z^2)\\ &= 8xy\Big(-8x^6y^2-8x^2y^6+8x^4y^4+(6x^4+6y^4-8x^2y^2)z^4\\ &\quad -6(x^2+y^2)z^6+(-6x^6-6y^6+2x^4y^2+2x^2y^4)z^2\Big),\end{aligned} \tag{A.11}$$

$$\begin{aligned}f_8(\boldsymbol{x}) &= f_5(\boldsymbol{x})(x^4+y^4+z^4)+f_6(\boldsymbol{x})(x^2+y^2+z^2)\\ &= 2x^{10}-6y^{10}-6z^{10}+10(x^8y^2+x^8z^2)+66(x^2y^8+x^2z^8)-6(y^8z^2+y^2z^8)\\ &\quad +68(x^6y^4+x^6z^4)-60(x^4y^6+x^4z^6)-6(y^6z^4+y^4z^6)\\ &\quad +80x^6y^2z^2+48x^2y^6z^2+48x^2y^2z^6-60x^4(y^4z^2+y^2z^4)+66x^2y^4z^4.\end{aligned} \tag{A.12}$$

Then we have

$$|f_1(\boldsymbol{x})| \le 2(x^2+y^2+z^2)^3, \tag{A.13}$$

$$|f_2(\boldsymbol{x})| \le \frac{7}{2}(x^2+y^2+z^2)^3, \tag{A.14}$$

$$|f_7(\boldsymbol{x})| \le 3(x^2+y^2+z^2)^5, \tag{A.15}$$

$$|f_8(\boldsymbol{x})| \le 6(x^2+y^2+z^2)^5. \tag{A.16}$$

Proof. Proof of (A.13) can be given with the following observation:

$$|8xy| \le 4(x^2+y^2). \tag{A.18}$$

For the first part, we make use of the Cauchy inequality:

$$x^6+y^6 \ge 2|x^3y^3| \quad \text{and} \quad 3(x^4y^2+x^2y^4) \ge 6|x^3y^3|,$$

so that

$$16|x^3y^3| \le 2(x^6+y^6+3x^4y^2+3x^2y^4) = 2(x^2+y^2)^3. \tag{A.19}$$

For the second part, we make the following observation:

$$\begin{aligned} 4(x^2+y^2)\left|-y^2z^2-x^2z^2+z^4\right| &\le 4(x^2+y^2)z^2(x^2+y^2+z^2) \\ &= 4(x^2+y^2)^2z^2+4(x^2+y^2)z^4. \end{aligned} \tag{A.20}$$

Therefore, a combination of (A.17), (A.19) and (A.20) yields

$$\begin{aligned} |f_1(\boldsymbol{x})| &\le 2(x^2+y^2)^3+4(x^2+y^2)^2z^2+4(x^2+y^2)z^4 \\ &\le 2(x^2+y^2+z^2)^3 = 2(x^2+y^2)^3+6(x^2+y^2)^2z^2+6(x^2+y^2)z^4+2z^6, \end{aligned} \tag{A.21}$$

so that inequality (A.14) is proved.

For $f_2(\boldsymbol{x})$, we first establish a lower bound:

$$f_2(\boldsymbol{x}) \ge -2y^6-2z^6-2(y^4z^2+y^2z^4) \ge -2(x^2+y^2+z^2)^3, \tag{A.22}$$

where the expansion (A.2) has been utilized. To obtain an upper bound for $f_2(\boldsymbol{x})$, we look at the following expansion:

$$\begin{aligned} &\frac{7}{2}(x^2+y^2+z^2)^3 - f_2(\boldsymbol{x}) \\ &\quad = \frac{3}{2}x^6+\frac{11}{2}(y^6+z^6)+\frac{9}{2}x^4(y^2+z^2)-\frac{15}{2}x^2(y^4+z^4)-3x^2y^2z^2 \\ &\qquad +\frac{25}{2}(y^4z^2+y^2z^4). \end{aligned} \tag{A.23}$$

Furthermore, an application of the Cauchy inequality indicates that

$$\frac{3}{4}x^4y^2+\frac{3}{4}y^2z^4 \ge \frac{3}{2}x^2y^2z^2, \quad \frac{3}{4}x^4z^2+\frac{3}{4}y^4z^2 \ge \frac{3}{2}x^2y^2z^2, \tag{A.24}$$

$$\frac{15}{4}y^6+\frac{15}{4}x^4y^2 \ge \frac{15}{2}x^2y^4, \quad \frac{15}{4}z^6+\frac{9}{2}x^4z^2 \ge \frac{15}{2}x^2z^4, \tag{A.25}$$

and its substitution into (A.23) leads to

$$\frac{7}{2}(x^2+y^2+z^2)^3 - f_2(\boldsymbol{x}) \ge 0, \tag{A.26}$$

so that an upper bound of $f_2(\boldsymbol{x})$ is available. As a result, (A.14) comes from a combination of the lower bound (A.22) and the upper bound (A.26).

To bound $f_7(\boldsymbol{x})$, we begin with the following decomposition:

$$|f_7(\boldsymbol{x})| \le Q^{(1)}+Q^{(2)}+Q^{(3)}+Q^{4)}, \tag{A.27}$$

where

$$\begin{aligned} Q^{(1)} &:= \left|64xy(-x^6y^2-x^2y^6+x^4y^4)\right|, \\ Q^{(2)} &:= \left|8xy(6x^4+6y^4-8x^2y^2)z^4\right|, \\ Q^{(3)} &:= \left|48xy(x^2+y^2)z^6\right|, \\ Q^{(4)} &:= \left|2xy(-8x^6-8y^6+9x^4y^2+9x^2y^4)z^2\right| \end{aligned}$$

so that

$$Q^{(1)} = 64|xy|(x^6y^2 + x^2y^6 - x^4y^4) = 64(|x^7y^3| + |x^3y^7| - |x^5y^5|). \tag{A.28}$$

Meanwhile, the following inequalities could be derived through repeated applications of the Cauchy inequality and Young's inequality:

$$5x^8y^2 + 10x^6y^4 \geq 10\sqrt{2}|x^7y^3|, \;\; x^{10} + \frac{32}{3}|x^5y^5| \geq \frac{5}{2}\cdot\left(\frac{64}{9}\right)^{3/5}|x^7y^3|, \tag{A.29}$$

which in turn yields

$$x^{10} + 5x^8y^2 + 10x^6y^4 + \frac{32}{3}|x^5y^5| \geq \left(10\sqrt{2} + \frac{5}{2}\cdot\left(\frac{64}{9}\right)^{3/5}\right)|x^7y^3|. \tag{A.30}$$

A similar inequality could be derived by a symmetry argument:

$$y^{10} + 5x^2y^8 + 10x^4y^6 + \frac{32}{3}|x^5y^5| \geq \left(10\sqrt{2} + \frac{5}{2}\cdot\left(\frac{64}{9}\right)^{3/5}\right)|x^3y^7|. \tag{A.31}$$

Then we arrive at

$$\begin{aligned} &x^{10} + y^{10} + 5(x^8y^2 + x^2y^8) + 10(x^6y^4 + x^4y^6) + \frac{64}{3}|x^5y^5| \\ &\quad \geq \left(10\sqrt{2} + \frac{5}{2}\cdot\left(\frac{64}{9}\right)^{3/5}\right)(|x^7y^3| + |x^3y^7|) \\ &\quad \geq \frac{64}{3}(|x^7y^3| + |x^3y^7|), \end{aligned} \tag{A.32}$$

where the last step comes from the fact that $10\sqrt{2} + \frac{5}{2}\cdot\left(\frac{64}{9}\right)^{3/5} \geq \frac{64}{3}$. This is equivalent to

$$3\Big(x^{10} + y^{10} + 5(x^8y^2 + x^2y^8) + 10(x^6y^4 + x^4y^6)\Big) \geq 64(|x^7y^3| + |x^3y^7| - |x^5y^5|) \geq Q^{(1)}. \tag{A.33}$$

For the second term $Q^{(2)}$, we make a similar observation:

$$6x^4 + 6y^4 - 8x^2y^2 \geq 0,$$

so that

$$Q^{(2)} = 8|xy|(6x^4 + 6y^4 - 8x^2y^2)z^4 \leq 8|xy|(6x^4 + 6y^4)z^4 = 48(|x^5y| + |xy^5|)z^4. \tag{A.34}$$

Meanwhile, the following inequality could be obtained with an application of Cauchy inequality:

$$10x^6z^4 + 30x^4y^2z^4 \geq 20\sqrt{3}|x^5y|z^4, \;\; 10y^6z^4 + 30x^2y^4z^4 \geq 20\sqrt{3}|xy^5|z^4, \tag{A.35}$$

which in turn implies that

$$Q^{(2)} \leq 48(|x^5y| + |xy^5|)z^4 \leq \frac{48}{20\sqrt{3}}(10x^6 + 10y^6 + 30x^4y^2 + 30x^2y^4)z^4. \tag{A.36}$$

Similar analysis could be applied to bound the third term $Q^{(3)}$: since

$$10x^4z^6 + 10x^2y^2z^6 \geq 20|x^3y|z^6 \quad \text{and} \quad 10y^4z^6 + 10x^2y^2z^6 \geq 20|xy^2|z^6,$$

it follows that

$$Q^{(3)} = \Big|48xy(x^2 + y^2)z^6\Big| = 48(|x^3y| + |xy^3|)z^6 \leq \frac{48}{20}\Big(10x^4z^6 + 10y^4z^6 + 20x^2y^2z^6\Big). \tag{A.37}$$

$$3(x^6+y^6)\geq 2\max(x^4y^2,x^2y^4),$$

indicates that

$$Q^{(4)}=\left|8xy(-6x^6-6y^6+2x^4y^2+2x^2y^4)z^2\right|\leq |8xy(6x^6+6y^6)z^2|=48(|x^7y|+|xy^7|)z^2. \tag{A.39}$$

Meanwhile, the following Cauchy inequalities are valid:

$$5x^8z^2+20x^6y^2z^2\geq 20|x^7y|z^2 \quad \text{and} \quad 5y^8z^2+20x^2y^6z^2\geq 20|xy^7|z^2. \tag{A.40}$$

These imply that

$$Q^{(4)}\leq 48(|x^7y|+|xy^7|)z^2\leq \frac{48}{20}\Big(5(x^8+y^8)z^2+20(x^6y^2+x^2y^6)z^2\Big). \tag{A.41}$$

A combination of (A.33), (A.34), (A.37), (A.41), together with the expansion (A.4) and the observation that $3\geq \max(\frac{48}{20},\frac{48}{20\sqrt{3}})$, results in the desired estimate (A.15).

To analyze $f_8(\boldsymbol{x})$, we first establish its lower bound. A careful calculation reveals that

$$\begin{aligned}
&6(x^2+y^2+z^2)^5+f_8(\boldsymbol{x})\\
&\quad=8x^{10}+40(x^8y^2+x^8z^2)+96(x^2y^8+x^2z^8)+24(y^8z^2+y^2z^8)\\
&\qquad+128(x^6y^4+x^6z^4)+54(y^6z^4+y^4z^6)\\
&\qquad+200x^6y^2z^2+168x^2y^6z^2+168x^2y^2z^6+120x^4(y^4z^2+y^2z^4)+246x^2y^4z^4\\
&\quad\geq 0.
\end{aligned} \tag{A.42}$$

To obtain its upper bound, we carry out a similar expansion:

$$\begin{aligned}
&6(x^2+y^2+z^2)^5-f_8(\boldsymbol{x})\\
&\quad=4x^{10}+12y^{10}+12z^{10}+20(x^8y^2+x^8z^2)-36(x^2y^8+x^2z^8)+36(y^8z^2+y^2z^8)\\
&\qquad-8(x^6y^4+x^6z^4)+120(x^4y^6+x^4z^6)+66(y^6z^4+y^4z^6)\\
&\qquad+40x^6y^2z^2+72x^2y^6z^2+72x^2y^2z^6+240x^4(y^4z^2+y^2z^4)+114x^2y^4z^4.
\end{aligned} \tag{A.43}$$

The following Cauchy inequalities,

$$9y^{10}+36x^4y^6\geq 36x^2y^8, \qquad 9z^{10}+36x^4z^6\geq 36x^2z^8, \tag{A.44}$$

$$4x^8y^2+4x^4y^6\geq 8x^6y^4, \qquad 4x^8z^2+4x^4z^6\geq 8x^6z^4, \tag{A.45}$$

when substituted into (A.43), imply that

$$6(x^2+y^2+z^2)^5-f_8(\boldsymbol{x})\geq 0. \tag{A.46}$$

Finally, a combination of (A.42) and (A.46) leads to the desired estimate (A.16). This completes the proof of Lemma A.1. □

Next, we proceed into the proof of Lemma 2.1.

Proof of Lemma 2.1. Based on the form for $\partial_{p_i} g^{(1)}$ in (2.4), careful calculations yield

$$g^{(1)}_{1,2}(\boldsymbol{p})=\frac{f_1(\boldsymbol{p})}{(p_1^2+p_2^2+p_3^2)^3}, \tag{A.47}$$

$$g^{(1)}_{1,1}(\boldsymbol{p})=\frac{f_2(\boldsymbol{p})}{(p_1^2+p_2^2+p_3^2)^3}. \tag{A.48}$$

The estimate $|g^{(1)}_{1,2}|\leq 2$ comes from the preliminary inequality (A.13), and the estimate $|g^{(1)}_{1,1}|\leq \frac{7}{2}$ is based on (A.14). The estimates for $|g^{(1)}_{1,3}|$, $|g^{(1)}_{2,3}|$, $|g^{(1)}_{2,2}|$ and $|g^{(1)}_{3,3}|$ could be handled by symmetry arguments.

Similarly, based on the form for $\partial_{p_i} g^{(2)}$ in (2.5), careful calculations give

The estimate $|g^{(2)}_{1,2}| \le 3$ comes from the preliminary inequality (A.15), and the estimate $|g^{(2)}_{1,1}| \le 6$ results from the inequality (A.16).

The estimates for $|g^{(2)}_{1,3}|$, $|g^{(2)}_{2,3}|$, $|g^{(2)}_{2,2}|$ and $|g^{(2)}_{3,3}|$ could be handled by symmetry arguments. This completes the proof of Lemma 2.1. □

Appendix B. Proof of Lemma 4.1

Proof of Lemma 4.1. For simplicity of presentation, we only focus on the first inequality (4.1); the other ones could be handled in the same manner. We assume that $\boldsymbol{p}_1 \neq \boldsymbol{p}_2$, since (4.1) is automatically satisfied otherwise. Define

$$\tilde{\boldsymbol{q}} := \boldsymbol{p}_2 - \boldsymbol{p}_1, \quad \boldsymbol{q} := \frac{\tilde{\boldsymbol{q}}}{L}, \quad L := |\tilde{\boldsymbol{q}}|,$$

so that $|\boldsymbol{q}| = 1$. If the line segment from $\boldsymbol{p}_1$ to $\boldsymbol{p}_2$ does not pass through the origin, $\mathbf{0}$, we observe that $\partial_{p_1} g^{(1)}$ is a smooth function over the whole line segment $\overrightarrow{\boldsymbol{p}_1\boldsymbol{p}_2}$, so that an application of the intermediate value theorem gives

$$\begin{aligned} \partial_{p_1} g^{(1)}(\boldsymbol{p}_1) - \partial_{p_1} g^{(1)}(\boldsymbol{p}_2) &= \nabla \partial_{p_1} g^{(1)}(\boldsymbol{p}_1 + \xi \boldsymbol{q}) \cdot \big(\boldsymbol{p}_1 - \boldsymbol{p}_2\big) \\ &= \sum_{j=1}^{3} g^{(1)}_{1,j}(\boldsymbol{p}_1 + \xi \boldsymbol{q}) \, [\boldsymbol{p}_1 - \boldsymbol{p}_2]_j \,, \end{aligned} \tag{B.1}$$

with for some $\xi \in [0, L]$. Estimate (4.1) is a direct consequence of (B.1), using the estimates for $g^{(1)}_{1,1}$, $g^{(1)}_{1,2}$ and $g^{(1)}_{1,3}$ given by (2.6) in Lemma 2.1.

On the other hand, in the case that the line segment $\overrightarrow{\boldsymbol{p}_1\boldsymbol{p}_2}$ does pass through the origin, $\mathbf{0}$, we parameterize the line in two segments. For the first, we use $\boldsymbol{p}_1 + t\boldsymbol{q}$, for $0 \le t \le L_1$, where $L_1 := |\boldsymbol{p}_1|$. Since $\partial_{p_1} g^{(1)}$ is continuous over $\mathbb{R}^3$ and differentiable over $\mathbb{R}^3_\star = \mathbb{R}^3 \backslash \mathbf{0}$, the intermediate value theorem can be applied between $\boldsymbol{p}_1$ and $\mathbf{0}$ and between $\mathbf{0}$ and $\boldsymbol{p}_2$, respectively:

$$\begin{aligned} \partial_{p_1} g^{(1)}(\boldsymbol{p}_1) - \partial_{p_1} g^{(1)}(\mathbf{0}) &= \nabla_p \partial_{p_1} g^{(1)}(\boldsymbol{p}_1 + \xi_1 \boldsymbol{q}) \cdot \boldsymbol{p}_1 \\ &= \sum_{j=1}^{3} g^{(1)}_{1,j}(\boldsymbol{p}_1 + \xi_1 \boldsymbol{q}) \, [\boldsymbol{p}_1]_j \,, \end{aligned} \tag{B.2}$$

$$\begin{aligned} \partial_{p_1} g^{(1)}(\mathbf{0}) - \partial_{p_1} g^{(1)}(\boldsymbol{p}_2) &= -\nabla_p \partial_{p_1} g^{(1)}(\boldsymbol{p}_1 + \xi_2 \boldsymbol{q}) \cdot \boldsymbol{p}_2 \\ &= -\sum_{j=1}^{3} g^{(1)}_{1,j}(\boldsymbol{p}_1 + \xi_2 \boldsymbol{q}) \partial_{p_j} \, [\boldsymbol{p}_2]_j \,, \end{aligned} \tag{B.3}$$

for some parameters $0 < \xi_1 < L_1$, $L_1 < \xi_2 < L$. Meanwhile, since $\overrightarrow{\boldsymbol{p}_1\boldsymbol{p}_2}$ passes through $\mathbf{0}$, we have

$$\boldsymbol{p}_1 = -\frac{L_1}{L}\tilde{\boldsymbol{q}}, \tag{B.4}$$

$$\boldsymbol{p}_2 = \frac{L - L_1}{L}\tilde{\boldsymbol{q}}. \tag{B.5}$$

Substitution into (B.2) – (B.3) reveals that

$$\partial_{p_1} g^{(1)}(\boldsymbol{p}_1) - \partial_{p_1} g^{(1)}(\boldsymbol{p}_2) = -\sum_{j=1}^{3} \Big(\frac{L_1}{L} g^{(1)}_{1,j}(\boldsymbol{p}_1 + \xi_1 \boldsymbol{q}) + \frac{L - L_1}{L} g^{(1)}_{1,j}(\boldsymbol{p}_1 + \xi_2 \boldsymbol{q}) \Big) \tilde{\boldsymbol{q}}. \tag{B.6}$$

Application of the estimates (2.6) for $g^{(1)}_{1,1}$, $g^{(1)}_{1,2}$ and $g^{(1)}_{1,3}$ yields the desired inequality (4.1), in the case that $\overrightarrow{\boldsymbol{p}_1\boldsymbol{p}_2}$ passes through $\mathbf{0}$.

Therefore, (4.1) is valid for any $\boldsymbol{p}_1$ and $\boldsymbol{p}_2$. The other inequalities could be analyzed in the same manner, and the details are skipped for the sake of brevity. □

References

[3] J. Boyd, Chebyshev and Fourier Spectral Methods, Dover, New York, NY, 2001.
[4] M. Burger, F. Haußer, C. Stöcker, A. Voigt, A level set approach to anisotropic flows with curvature regularization, J. Comput. Phys. 225 (2007) 183–205.
[5] J.W. Cahn, On spinodal decomposition, Acta Metall. 9 (1961) 795.
[6] J.W. Cahn, J.E. Hilliard, Free energy of a nonuniform system. I. Interfacial free energy, J. Chem. Phys. 28 (1958) 258–267.
[7] J.W. Cahn, D.W. Hoffman, A vector thermodynamics for anisotropic surfaces-II, curved and faceted surfaces, Acta Metall. 22 (1974) 1205–1214.
[8] C. Canuto, A. Quarteroni, Approximation results for orthogonal polynomials in Sobolev spaces, Math. Comput. 38 (1982) 67–86.
[9] C. Chen, X. Yang Fast, Provably unconditionally energy stable, and second-order accurate algorithms for the anisotropic Cahn-Hilliard model, Comput. Methods Appl. Mech. Eng. 351 (2019) 35–59.
[10] F. Chen, J. Shen, Efficient energy stable schemes with spectral discretization in space for anisotropic Cahn-Hilliard systems, Commun. Comput. Phys. 13 (2013) 1189–1208.
[11] W. Chen, S. Conde, C. Wang, X. Wang, S.M. Wise, A linear energy stable scheme for a thin film model without slope selection, J. Sci. Comput. 52 (2012) 546–562.
[12] W. Chen, W. Feng, Y. Liu, C. Wang, S.M. Wise, A second order energy stable scheme for the Cahn-Hilliard-Hele-Shaw equation, Discrete Contin. Dyn. Syst., Ser. B 24 (1) (2019) 149–182.
[13] W. Chen, Y. Liu, C. Wang, S.M. Wise, An optimal-rate convergence analysis of a fully discrete finite difference scheme for Cahn-Hilliard-Hele-Shaw equation, Math. Comput. 85 (2016) 2231–2257.
[14] W. Chen, C. Wang, X. Wang, S.M. Wise, A linear iteration algorithm for energy stable second order scheme for a thin film model without slope selection, J. Sci. Comput. 59 (2014) 574–601.
[15] W. Chen, C. Wang, X. Wang, S.M. Wise, Positivity-preserving, energy stable numerical schemes for the Cahn-Hilliard equation with logarithmic potential, J. Comput. Phys.: X 3 (2019) 100031.
[16] Y. Chen, M. Huang, Simulating three-dimensional nanocrystal faceting using a regularized, strongly anisotropic Cahn-Hilliard model, Commun. Comput. Phys. (2019), submitted for publication.
[17] Y. Chen, J.S. Lowengrub, J. Shen, C. Wang, S.M. Wise, Efficient energy stable schemes for isotropic and strongly anisotropic Cahn-Hilliard systems with the Willmore regularization, J. Comput. Phys. 365 (2018) 57–73.
[18] K. Cheng, W. Feng, S. Gottlieb, C. Wang, A Fourier pseudospectral method for the “Good” Boussinesq equation with second-order temporal accuracy, Numer. Methods Partial Differ. Equ. 31 (1) (2015) 202–224.
[19] K. Cheng, W. Feng, C. Wang, S.M. Wise, An energy stable fourth order finite difference scheme for the Cahn-Hilliard equation, J. Comput. Appl. Math. 362 (2019) 574–595.
[20] K. Cheng, Z. Qiao, C. Wang, A third order exponential time differencing numerical scheme for no-slope-selection epitaxial thin film model with energy stability, J. Sci. Comput. 81 (1) (2019) 154–185.
[21] K. Cheng, C. Wang, Long time stability of high order multi-step numerical schemes for two-dimensional incompressible Navier-Stokes equations, SIAM J. Numer. Anal. 54 (2016) 3123–3144.
[22] K. Cheng, C. Wang, S.M. Wise, X. Yue, A second-order, weakly energy-stable pseudo-spectral scheme for the Cahn-Hilliard equation and its solution by the homogeneous linear iteration method, J. Sci. Comput. 69 (2016) 1083–1114.
[23] A. DiCarlo, M. Gurtin, P. Podio-Guidugli, A regularized equation for anisotropic motion-by-curvature, SIAM J. Appl. Math. 52 (1992) 1111–1119.
[24] A. Diegel, X. Feng, S.M. Wise, Convergence analysis of an unconditionally stable method for a Cahn-Hilliard-Stokes system of equations, SIAM J. Numer. Anal. 53 (2015) 127–152.
[25] A. Diegel, C. Wang, X. Wang, S.M. Wise, Convergence analysis and error estimates for a second order accurate finite element method for the Cahn-Hilliard-Navier-Stokes system, Numer. Math. 137 (2017) 495–534.
[26] A. Diegel, C. Wang, S.M. Wise, Stability and convergence of a second order mixed finite element method for the Cahn-Hilliard equation, IMA J. Numer. Anal. 36 (2016) 1867–1897.
[27] L. Dong, W. Feng, C. Wang, S.M. Wise, Z. Zhang, Convergence analysis and numerical implementation of a second order numerical scheme for the three-dimensional phase field crystal equation, Comput. Math. Appl. 75 (6) (2018) 1912–1928.
[28] J.J. Eggleston, G.B. McFadden, P.W. Voorhees, A phase-field model for highly anisotropic interfacial energy, Physica D 150 (2001) 91–103.
[29] D. Eyre, Unconditionally gradient stable time marching the Cahn-Hilliard equation, in: J.W. Bullard, R. Kalia, M. Stoneham, L.Q. Chen (Eds.), Computational and Mathematical Models of Microstructural Evolution, vol. 53, Materials Research Society, Warrendale, PA, USA, 1998, pp. 1686–1712.
[30] W. Feng, A.J. Salgado, C. Wang, S.M. Wise, Preconditioned steepest descent methods for some nonlinear elliptic equations involving p-Laplacian terms, J. Comput. Phys. 334 (2017) 45–67.
[31] X. Feng, S.M. Wise, Analysis of a fully discrete finite element approximation of a Darcy-Cahn-Hilliard diffuse interface model for the Hele-Shaw flow, SIAM J. Numer. Anal. 50 (2012) 1320–1343.
[32] D. Gottlieb, S.A. Orszag, Numerical Analysis of Spectral Methods, Theory and Applications, SIAM, Philadelphia, PA, 1977.
[33] S. Gottlieb, F. Tone, C. Wang, X. Wang, D. Wirosoetisno, Long time stability of a classical efficient scheme for two dimensional Navier-Stokes equations, SIAM J. Numer. Anal. 50 (2012) 126–150.
[34] S. Gottlieb, C. Wang, Stability and convergence analysis of fully discrete Fourier collocation spectral method for 3-d viscous Burgers’ equation, J. Sci. Comput. 53 (2012) 102–128.
[35] Z. Guan, J.S. Lowengrub, C. Wang, Convergence analysis for second order accurate schemes for the periodic nonlocal Allen-Cahn and Cahn-Hilliard equations, Math. Methods Appl. Sci. 40 (18) (2017) 6836–6863.
[36] Z. Guan, J.S. Lowengrub, C. Wang, S.M. Wise, Second-order convex splitting schemes for nonlocal Cahn-Hilliard and Allen-Cahn equations, J. Comput. Phys. 277 (2014) 48–71.
[37] Z. Guan, C. Wang, S.M. Wise, A convergent convex splitting scheme for the periodic nonlocal Cahn-Hilliard equation, Numer. Math. 128 (2014) 377–406.
[38] J. Guo, C. Wang, S.M. Wise, X. Yue, An H^2 convergence of a second-order convex-splitting, finite difference scheme for the three-dimensional Cahn-Hilliard equation, Commun. Math. Sci. 14 (2016) 489–515.
[39] J. Hesthaven, S. Gottlieb, D. Gottlieb, Spectral Methods for Time-Dependent Problems, Cambridge University Press, Cambridge, UK, 2007.
[40] Z. Hu, S. Wise, C. Wang, J. Lowengrub, Stable and efficient finite-difference nonlinear-multigrid schemes for the phase-field crystal equation, J. Comput. Phys. 228 (2009) 5323–5339.
[41] R. Kobayashi, Modeling and numerical simulations of dendritic crystal growth, Physica D 63 (1993) 410–423.
[42] Y. Liu, W. Chen, C. Wang, S.M. Wise, Error analysis of a mixed finite element method for a Cahn-Hilliard-Hele-Shaw system, Numer. Math. 135 (2017) 679–709.
[43] A. Makki, A. Miranville, Existence of solutions for anisotropic Cahn-Hilliard and Allen-Cahn systems in higher space dimensions, Discrete Contin. Dyn.

[47] R.F. Sekerka, Analytical criteria for missing orientations on three-dimensional equilibrium shapes, J. Cryst. Growth 275 (2005) 77–82.
[48] E.J. Siem, W.C. Carter, Orientation-dependent surface tension functions for surface energy minimizing calculations, J. Mater. Sci. 40 (2005) 3107–3113.
[49] J.E. Taylor, J.W. Cahn, Diffuse interface with sharp corners and facets: phase field models with strongly anisotropic surfaces, Physica D 112 (1998) 381–411.
[50] S. Torabi, J.S. Lowengrub, Simulating interfacial anisotropy in thin-film growth using an extended Cahn-Hilliard model, Phys. Rev. E 85 (2012) 041603.
[51] S. Torabi, J.S. Lowengrub, A. Voigt, S.M. Wise, A new phase-field model for strongly anisotropic systems, Proc. R. Soc. Lond., Ser. A, Math. Phys. Eng. Sci. 465 (2009) 1337–1359.
[52] C. Wang, X. Wang, S.M. Wise, Unconditionally stable schemes for equations of thin film epitaxy, Discrete Contin. Dyn. Sys. A 28 (2010) 405–423.
[53] C. Wang, S.M. Wise, An energy stable and convergent finite-difference scheme for the modified phase field crystal equation, SIAM J. Numer. Anal. 49 (2011) 945–969.
[54] A.A. Wheeler, Phase-field theory of edges in an anisotropic crystal, Proc. R. Soc. A 462 (2006) 3363–3384.
[55] S.M. Wise, Unconditionally stable finite difference, nonlinear multigrid simulation of the Cahn-Hilliard-Hele-Shaw system of equations, J. Sci. Comput. 44 (2010) 38–68.
[56] S.M. Wise, J.S. Kim, J.S. Lowengrub, Solving the regularized, strongly anisotropic Chan-Hilliard equation by an adaptive nonlinear multigrid method, J. Comput. Phys. 226 (2007) 414–446.
[57] S.M. Wise, C. Wang, J.S. Lowengrub, An energy stable and convergent finite-difference scheme for the phase field crystal equation, SIAM J. Numer. Anal. 47 (2009) 2269–2288.
[58] Y. Yan, W. Chen, C. Wang, S.M. Wise, A second-order energy stable BDF numerical scheme for the Cahn-Hilliard equation, Commun. Comput. Phys. 23 (2018) 572–602.
[59] J. Zhang, C. Chen, X. Yang, Y. Chu, Z. Xia, Efficient, non-iterative, and second-order accurate numerical algorithms for the anisotropic Allen-Cahn equation with precise nonlocal mass conservation, J. Comput. Appl. Math. 363 (2019) 444–463.